Journal of Wind Engineering & Industrial Aerodynamics 219 (2021) 104805

Contents lists available at ScienceDirect

Journal of Wind Engineering & Industrial Aerodynamics

journal homepage: www.elsevier.com/locate/jweia

The use of a Laguerrian expansion basis as Volterra kernels for the efficient modeling of nonlinear self-excited forces on bridge decks

Henrik Skyvulstad [a,b,*], Øyvind W. Petersen [b], Tommaso Argentini [c], Alberto Zasso [c], Ole Øiseth [b]

[a] Bridge Department, Norconsult AS, Sandvika, Norway
[b] Department of Structural Engineering, Norwegian University of Science and Technology, Trondheim, Norway
[c] Department of Mechanical Engineering, Politecnico di Milano, Milano, Italy

ARTICLE INFO

Keywords:
Aeroelasticity
Nonlinear
Volterra models
Bridge aerodynamics
Double deck

ABSTRACT

In the last decade, the bridge aerodynamics community has pivoted towards the investigation and prediction of nonlinear aerodynamic phenomena. Several nonlinear models have been suggested, but the research community has yet to conclude on the best types of models for the wide range of nonlinearity observed in the research. Multiple authors have indicated that Volterra models show promise in modeling nonlinear bridge aerodynamics. However, efficient data-driven identification of the Volterra model is challenging. A Laguerrian expansion basis is introduced in this work to alleviate the identification issue. The proposed method improves the identification of the Volterra models, leading to a reduction in computational effort and simplification of the least-squares problem by parameterizing the kernels. The method is also more robust to noise and small perturbations in the experimental data, leading to smooth, decaying kernels that are interpretable in a physical context. A relevant theoretical example is given to evaluate the applicability of the technique in bridge aerodynamics. Furthermore, the method is used to identify 1st^{-} to 4th-order Volterra models on the experimental data of one degree of freedom and two degrees of freedom self-excited forces. The study shows that the technique can identify Volterra models with high fidelity when one degree of freedom and most two degrees of freedom motion data are considered. The model struggles slightly when considering the noisiest and most nonlinear two degrees of freedom scenarios for self-excited drag force.

1. Introduction

Wind loading often governs the dynamic behavior of long-span bridges. Thus, the interaction between the bridge and the wind has been an avid research topic of interest. Twin deck configurations have become a standard solution to avoid aerodynamic instabilities for bridges with super long spans. However, wind tunnel tests have shown that twin deck cross-sections often exhibit nonlinear aerodynamic behavior (Diana et al., 2004; Skyvulstad et al., 2017; Zhang et al., 2017; Zhou et al., 2018b, 2019a). Numerous methods have been proposed to adequately capture the nonlinear effects of unsteady forces, but no specific model has been shown to prevail (Abbas et al., 2020; Chen and Kareem, 2001, 2003; Chen et al., 2020; Diana et al., 1993, 1995, 2008, 2010, 2013; Diana and Omarini, 2020; Gao et al., 2018; Gao and Zhu, 2017; Wu and Kareem, 2011, 2013a; Zhang et al., 2020; Zhou et al., 2018a, 2019a, 2019b).

The Volterra series model is a general nonlinear model that expands linear convolutions to higher-order convolutions (Schetzen, 1980; Volterra, 1959). The Volterra series model can be thought of as a Taylor series with a memory. An extensive review of the different identification methods and the use of the Volterra series models in the research community can be found in (Cheng et al., 2017). The functionality of such models for bridge aerodynamics applications has been explored in the time domain (Ali et al., 2020; Denoël and Carassale, 2015; Wu and Kareem, 2013b, 2013c, 2014, 2015a, 2015b) and the frequency domain (Carassale et al., 2014; Carassale and Kareem, 2010).

Volterra series model applications in bridge aerodynamics have been mainly based on identification from the theoretical expressions of nonlinear systems or data-driven identification by sparse or full pseudoinverse identification. The use of data-driven identification methods of the Volterra series is still not extensively explored in the bridge aerodynamics research community. The efficient identification of Volterra series models has been a research topic since the 1950s (Wiener, 1958). Wiener proposed the Wiener series with orthogonal Wiener

* Corresponding author. Bridge Department, Norconsult AS, Sandvika, Norway.
E-mail address: henrik.skyvulstad@ntnu.no (H. Skyvulstad).

https://doi.org/10.1016/j.jweia.2021.104805
Received 22 February 2021; Received in revised form 1 October 2021; Accepted 9 October 2021
Available online 18 October 2021

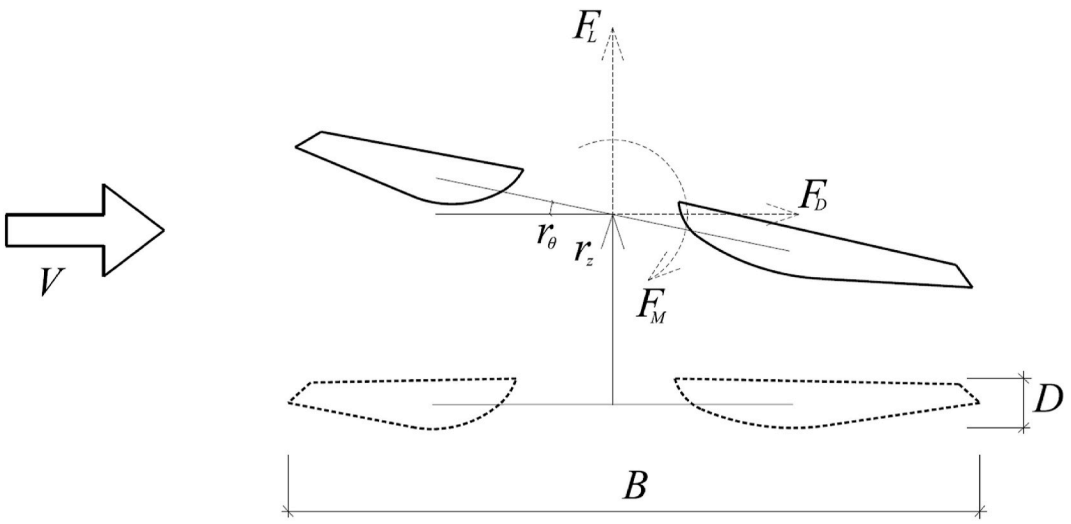

Fig. 1. Force and motion definitions.

kernels. This method is based on a Gram-Schmidt orthogonalization of the Volterra kernels assuming Gaussian white noise as the training input (Lee and Schetzen, 1965). developed an efficient algorithm for identifying Wiener kernels by a cross-correlation-based method, but the training data input was still restricted to Gaussian white noise (Korenberg and Hunter, 1990). developed the repeated Toeplitz inversion algorithm for identifying a Weiner series with Gaussian colored noise as input. Other efforts have been made to identify Volterra kernels (Delport, 2005): identified Volterra kernels by a tailored sequence of impulse inputs with varying amplitudes and time separations (Wray and Green, 1994). recognized that kernels could be identified through a rewriting of the unknowns in an artificial neural network (Batselier et al., 2019). used a tensor network iterative algorithm to identify the kernels.

One issue with the Volterra series models is the curse of dimensionality, where the computational burden increases rapidly with the number of inputs, the model order and memory length. One way to alleviate this problem is to use a parameterized kernel expanded by basis functions with relatively few coefficients. Utilizing a parameterized kernel for the Volterra series was first suggested by (Wiener, 1958), who suggested simple time-delay functions as a basis, which was first implemented by (Watanabe and Stark, 1975). The solution was also recognized by (Amorocho, J., Brandstetter, 1971), who recast the identification problem into a linear least squares regression problem (Korenberg, 1987). proposed an ordinary orthogonal algorithm and further proposed the fast-orthogonal algorithm (FOA) to solve the least-squares regression problem more efficiently.

While the use of parameterized kernels brings computational benefits, a remaining challenge is to find suitable low-order expansions that can properly represent the physical fluid memory effects in the context of bridge aerodynamics (Prazenica, 2002). used a set of wavelet functions as the expansion basis. The wavelet expansion basis has been used in the aerospace community (Khawar et al., 2012). (Reisenthel, 1999) suggested exponential decay, while (Nelles, 2001; Seretis and Zafirioul, 1997) suggested distorted sine functions as filter banks (Ogura, 1986). worked with the Laguerrian expansion basis but tried to identify the coefficients through a cross-correlation method (Marmarelis, 1993). developed the method further and recast the identification into a least-squares problem. Using a Laguerrian expansion basis, the kernels can be parameterized by considering a superposition of a given number of filters as basis functions. In a model identification context, the most significant benefit from using a parameterized model is that the number of unknown coefficients is significantly reduced.

Fewer unknown coefficients make the identification problem less computationally expensive and reduce the model's necessary training data. Less computationally expensive operations open the opportunity to identify higher-order and multiple input Volterra models. As will be shown, the number of unknown Laguerrian coefficients is independent of the memory length, which can be set as arbitrarily long, thus allowing for long memory and utilizing high sampling frequencies. As will be shown, a high sampling frequency can be important when the identified Volterra series model in nondimensional time is rescaled for full-scale time-domain simulations. The Laguerrian filters are mutually orthonormal, and the filter coefficients become orthogonal for white noise inputs or nearly orthogonal for colored noise inputs, which makes the identification process better conditioned (Westwick and Kearney, 2003). The filters decay to zero, which is the case for most physical systems. The filters also have a low-pass filter property that suppresses higher-order noise, making the kernel smoother than classic pseudoinverse identification. The physical interpretation of the kernel thus becomes more straightforward.

To the best of the author's knowledge, the Laguerrian expansion has not yet been explored in the bridge aerodynamics community. In this paper, the Laguerrian expansion technique is used to estimate the Volterra kernels to predict nonlinear motion-induced forces on bridge decks. The technique's effectiveness is demonstrated in a numerical example and with experimental data from state-of-the-art wind tunnel tests. The theory and experimental application are also extended to systems with multiple inputs. The experimental data stems from forced vibration tests with relatively low amplitude pitching motion and combined pitching and vertical motion. The nonlinearity of the section forces varies from significant for the drag force, mildly nonlinear for the pitching moment, and linear for the lift force. Modelling of the drag force using Volterra models is the main focus of this work.

2. Nonlinear bridge aerodynamics

Nonlinearity is an inherent property of fluid dynamics and can manifest itself in many forms. The most relevant nonlinearities in bridge aerodynamics are amplitude dependency and harmonic distortion. Traditionally, bridge engineers strive to design bridge cross-sections that behave mostly linear within the bridge operating range. Furthermore, design codes often specify a minimum flutter onset speed, without designing for post-flutter responses. It is well known that vortex-induced vibration is self-limiting, but most design codes place restrictions on the onset and not the response amplitude.

Significant research efforts are being placed into modeling nonlinear aerodynamic phenomena. It is important to note that nonlinearity is not necessarily unfavorable. Several of the different phenomena assumed to

Fig. 2. Identification problem for self-excited force modelling. F could be drag force, lift force or pitching moment.

have unbounded responses in a linear analysis are in reality bounded by nonlinear limit-cycle oscillations (LCOs). By utilizing the actual nonlinearity of the problem and not restricting and assuming the phenomena to be linear, one opens the opportunity to build longer and safer bridges at a lower cost. To do so, we need robust and well-documented nonlinear load models and ways to correctly identify these models.

A suitable nonlinear model should be user-friendly and flexible enough to describe a broad range of nonlinear behaviors. The model should also be easily identified with appropriate engineering tools such as computational fluid dynamics (CFD), perturbations of theoretical models or wind tunnel experiments. In this work, a data-driven identification technique using input-output data at successive time intervals is used to identify the model.

Fig. 1 shows a bridge section model subjected to wind with a mean wind speed V. The vertical and pitching motions of the model are denoted as r_z and r_θ, and the self-excited drag and lift forces and pitching moments are denoted as F_D, F_L, and F_M. Fig. 2 shows an overview of the identification problem for modeling nonlinear self-excited forces with vertical and pitching motion as inputs. Separate systems can model the self-excited drag, lift and pitching moment, and it should also be noted that the horizontal motion can be added to the framework straightforwardly. Since the self-excited drag force due to vertical and pitching motions shows the most interesting nonlinear aerodynamic behavior, for the forces considered, the main focus in this paper is given to the drag force.

Research on nonlinear self-excited forces on bridges has mainly focused on lift and pitching moment, since these are the typical drivers of LCOs for galloping, vortex-induced vibrations, and nonlinear flutter. The drag force will often exhibit nonlinearities even for relatively small amplitudes due to the quadratic shape of the drag coefficient. Wind tunnel tests of the streamlined bridge decks clearly show 2nd-order effects of the drag component (Siedziako and Øiseth, 2018). The nonlinearities could be one reason why a large scatter is often observed for the aerodynamic derivatives relating to the drag force. These observations indicate that the traditional quasi-steady theory will not accurately predict the aerodynamic damping from drag. On the other hand, nonlinear models could improve the drag force prediction needed in simulations of bridge responses to wind loading. The self-excited forces from Volterra series convolutions can be incorporated into standard numerical integration techniques for nonlinear time-domain simulations. However, such aeroelastic system simulations of bridge responses are outside the scope of this contribution, and only the modelling of the self-excited forces is considered here.

In the wind tunnel tests in this paper, a relatively low motion amplitude is used (less than 3° for the pitching motion), which roughly corresponds to the displacement of a bridge in the ultimate limit state. As a simplification of the multi-modal buffeting response of the bridge decks, broad-banded stochastic motion is used to identify the model. This is an efficient way to incorporate multiple frequencies and amplitudes in the input motion. The Volterra model could also be used to evaluate the LCOs, which typically display a single or double harmonic motion behavior with large amplitudes (Gao et al., 2020; Zhang et al., 2020). Large-amplitude harmonic motions should be used in the training data for accurate modelling and identification of these phenomena. Evaluation of Volterra models for these effects is also outside the scope but would be an interesting study for the future.

After a model is identified, a new set of inputs can in principle be fed through the model to predict the self-excited force. One should however be very careful to extrapolate with the nonlinear models; one can generally only the model prediction to perform well for input motions that are relatively similar to those considered in the model identification. This is because the model is not necessarily able to generalize outside the domain of the training data.

The next chapter explains how nonlinear aerodynamic forces for bridge decks can be modeled using Volterra models. The aerodynamic forces may depend nonlinearly on incoming turbulence, bridge motion, or a combination of both. This paper focuses on modeling nonlinearities stemming from bridge motion, but the method could easily be used on nonlinearities stemming from turbulence.

3. Volterra model

The Volterra series model of order p for causal single-input-single-output systems can be formulated in a continuous time-domain form as follows (Rugh, 1981):

$$F = h_0 + \int_0^t h_1(t-\tau)r(\tau)d\tau + \sum_{P=2}^{p}\int_0^t \dots \int_0^t \int_0^t h_P(t-\tau_1,\dots,t - \tau_P)r(\tau_1)\dots r(\tau_P)d\tau_1\dots d\tau_P \quad (1)$$

Here, h_p is the pth-order Volterra kernel. Furthermore, r is the input of the system (usually horizontal, vertical or pitching motion in the context of bridge aerodynamics), and F is the system output, which in our case is the self-exited drag, lift or pitching motion. By introducing the assumption that the system has finite fading memory with memory length M, the discrete form of the Volterra series model becomes (Clancy and Rugh, 1979):

$$F[n] = h_0 + \sum_{k=0}^{M} h_1[k]r[n-k] + \sum_{P=2}^{p} H_M^P[n] \quad (2)$$

$$H_M^p[n] = \sum_{k_1}^{M}\dots\sum_{k_p}^{M} h_p[k_1,\dots,k_p]r[n-k_1]\dots r[n-k_p] \quad (3)$$

For 2nd-order models ($p = 2$), a multi-input-single-output (MISO) system with two inputs can be described as follows:

$$F[n] = h_0 + \sum_{k=0}^{M} h_1^{r_1}[k]r_1[n-k] + \sum_{k=0}^{M} h_1^{r_2}[k]r_2[n-k] + \dots$$
$$\sum_{k_1=0}^{M}\sum_{k_2=0}^{M} h_2^{r_1r_1}[k_1,k_2]r_1[n-k_1]r_1[n-k_2] + \sum_{k_1=0}^{M}\sum_{k_2=0}^{M} h_2^{r_2r_2}[k_1,k_2]r_2[n-k_1]r_2[n-k_2] \quad (4)$$

Here, $h_2^{r_1r_1}[k_1,k_2]$ and $h_2^{r_2r_2}[k_1,k_2]$ are called the 2nd-order direct kernels, while $h_2^{r_1r_2}[k_1,k_2]$ and $h_2^{r_2r_1}[k_1,k_2]$ are denoted as cross-kernels. For high model orders (p) and long memory lengths (M), the number of unknown kernel coefficients to be identified becomes very large. A large number of coefficients increases the computational burden and requires more input/output data for statistical confidence in the unknown coefficients. One way to reduce the number of coefficients is to use a parameterized kernel using basis functions/filters. In the following, attention is given to the Laguerre expansion basis (Marmarelis, 1993). As will be explained, the parameters of the Laguerre filters can be identified utilizing least squares, which provides a relatively loose constraint on the type of input to the dynamic system, and one could use a reasonably wide input range as long as a sufficiently high dynamic order is used (Marmarelis, 1993).

The impulse response functions (IRFs) for the discrete Laguerrian filters are defined by (Marmarelis, 1993):

$$g_l[k] = \alpha^{(k-l)/2}(1-\alpha)^{(1/2)}\sum_{i=0}^{l}(-1)^i\binom{k}{i}\binom{l}{i}\alpha^{l-i}(1-\alpha)^i, \quad k \geq 0 \quad (5)$$

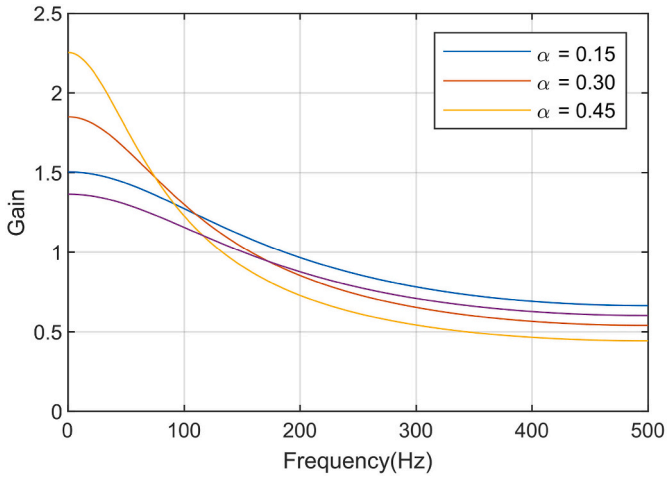

Fig. 3. Gain of Laguerre filters with different decay factors. Note that the gain is independent of the filter order.

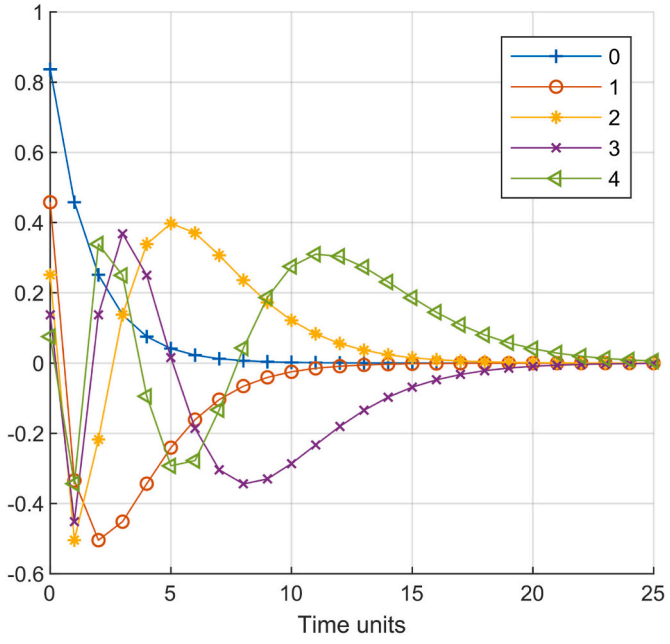

Fig. 4. Time-domain plot of different Laguerre filter orders with α = 0.3. Note that the number of zero crossings is equal to the filter order.

where $l = 0 \ldots J$ is the filter number. The functions $g_l[k]$ approach zero for large k values at a rate controlled by a single parameter, the decay parameter $0 < \alpha < 1$. As will be shown later, the Volterra kernels are constructed as a summation of multiplications of the Laguerre IRFs:

$$h_1[k] = \sum_{l=0}^{J} c_l g_l[k] \tag{6}$$

$$\mathbf{h}_P[k_1, \ldots, k_p] = \sum_{l_1=0}^{J} \cdots \sum_{l_p=0}^{J} c_{l_1 \ldots l_p} \left(g_{l_1}[k_1] \ldots g_{l_p}[k_p] \right), \quad p > 1 \tag{7}$$

where c represents unknown constant coefficients. The determination of the constant coefficients in Eq. (6)–(7) and (15)–(16) are discussed in Chapter 3.1.

It can be shown that the z-transform of Eq. (5) is given by:

$$G_l(z) = \left(\frac{\sqrt{\alpha} - z^{-1}}{1 - \sqrt{\alpha} z^{-1}} \right)^l \left(\frac{\sqrt{1-\alpha}}{1 - \sqrt{\alpha} z^{-1}} \right) \tag{8}$$

Note that the gain of these frequency response functions is independent of the filter number l:

$$|G_l(z)| = \left| \frac{\sqrt{1-\alpha}}{1 - \sqrt{\alpha} z^{-1}} \right| \tag{9}$$

Here, α controls the cutoff frequency, as this basis function acts as a low-pass filter. The choice of this parameter is discussed later. In this paper, the decay parameter is restricted to be equal for all filter and model orders. For a more general description of the Laguerre expansion basis technique, this need not be the case (Israelsen and Smith, 2014).

Fig. 3 and Fig. 4 show frequency and time-domain properties of different Laguerre filters. Fig. 3 shows Eq. (9) and the effect of α on the low-pass filter properties of the model. Fig. 4 shows the time-domain properties of the IRF of the filters, and it is interesting to note that the filter order is equal to the number of zero-crossings of the IRF. Additional properties of the filters as modelling of time delays, length of memory depends on the decay factor and phase properties of the filters can be found in (Marmarelis, 1993).

3.1. Identifying procedure

To structure the least-squares problem for kernel identification, one can follow these steps (Westwick and Kearney, 2003):

1. Choose a suitable number of filters $g_l[k]$, $l = 0 \ldots J$
2. Compute the outputs of each filter via convolution of the inputs:

$$x_l[n] = \sum_{k=0}^{M} g_l[k] r[n-k] \quad for\ l = 0 \ldots J \tag{10}$$

3. Construct the regression matrix,

$$\mathbf{X}[n, :] = \left[1\ x_0[n] \ldots x_J[n]\ x_0^2[n]\ x_0[n] x_1[n] \ldots x_J^2[n]\ \ldots\ x_J^P[n] \right] \tag{11}$$

Higher-order and cross terms can easily be obtained by adding additional columns.

4. Solve the least-squares problem:

$$F = \mathbf{X}\theta \tag{12}$$

where θ is the coefficient vector to be solved by linear least-squares. F is the output vector. The kernels can further be constructed from the estimated coefficient vector S using the following relations:

$$\widehat{\theta} = \left[\bar{c}_0\ |c_0 \ldots c_J\ |\ c_{0,0}\ \ldots\ c_{J,J}\ |c_{0,0,0} \ldots c_{J,J,J}|\ c_{0,\ldots,0} \ldots c_{J,\ldots,J} \right]^{\mathrm{T}} \tag{13}$$

$$h_0 = \bar{c}_0 \tag{14}$$

$$h_1[k] = \sum_{l=0}^{J} c_l g_l[k] \tag{15}$$

$$\mathbf{h}_P[k_1, \ldots, k_p] = \sum_{l_1=0}^{J} \cdots \sum_{l_p=0}^{J} c_{l_1 \ldots l_p} \left(g_{l_1}[k_1] \ldots g_{l_p}[k_p] \right), \quad p > 1 \tag{16}$$

To further improve the identification efficiency, one can utilize the recursive relation to make the single columns in the regressor matrix $\mathbf{X}$. The recursive relation is given according to (Ogura, 1986):

$$x_0[n] = \sqrt{\alpha} x_0[n-1] + \sqrt{1-\alpha} r[n], \quad x_0[0] = 0 \tag{17}$$

$$x_l[n] = \sqrt{\alpha} x_l[n-1] + \sqrt{\alpha} x_{l-1}[n] - x_{l-1}[n-1], \quad l = 1 \ldots J, \quad x_l[0] = 0 \tag{18}$$

By using these recursive equations the entire available motion history is implicitly considered. This means that the truncation introduced by only considering the first M points of the filters have been removed. The effective memory of the IRFs is entirely determined by the decay factor with an effective total memory length according to the total length of the longest stretching filter. As indicated in Fig. 4, the Laguerre IRFs approach zero, where the highest-order filter always stretches the furthest. For the Laguerre expansion basis, the number of unknown coefficients is given by:

$$C_{(p,J)} = \frac{(J+1)^{p+1}-1}{J} \simeq J^p \tag{19}$$

For comparison, the number of parameters that need to be determined in the full (non-parametrized) Volterra series model is given by:

$$C_{(p,M)} = \frac{(M+1)^{p+1}-1}{M} \simeq M^p \tag{20}$$

Thus, for high-order models where the number of filters is smaller than the memory length ($J < M$), the reduction in computational burden requirements can be significant. Note that additional redundancies can be removed by considering the well-known symmetry of the higher-order kernels. High sampling rates give a high necessary memory length, making the model computationally intensive to identify. For long necessary memory lengths, the Laguerrian expansion basis has a considerable advantage, especially as shown in the next chapter.

The Laguerrian filters are orthonormal over the interval between (0,∞) because they follow the relation:

$$\sum_{k=0}^{\infty} g_m[k]g_n[k] = \delta_{nm} = \begin{cases} 0 & for\ m \neq n \\ 1 & for\ m = n \end{cases} \tag{21}$$

Orthonormality implies that the Laguerrian filters are uncorrelated with each other, which in turn makes for a well-conditioned identification problem. When the system input is Gaussian white noise, the filter coefficients in Eq. (13) also become uncorrelated. This further implies that if one has identified a Volterra model with a given set of filters, one can add a filter and only expect the coefficient for that filter to change. Furthermore (Marmarelis, 1993), concluded that the input does not need to be Gaussian white noise as long as all of the system frequencies are excited, and a high enough order is included in the model (Marmarelis, 1993). stated that the coefficients are said to be near orthonormal under these circumstances. The filter coefficients are found through least-squares identification, without any restriction on the type of input. This means that using single-harmonic inputs or harmonic sweeps is also applicable for training the model, with the condition that the model only is valid for the frequency and amplitude range of the training data.

3.2. Determination of the decay parameter α

For a given filter order *J,* the decay parameter α remains to be determined. The decay parameter controls the potential effective memory of the model, but as illustrated in Fig. 4 it is the sum of the filters for all orders that control the actual shape of the kernel. Many different decay factors have been tested by the authors, and our experience is that the methodology generally is robust both in terms of model identification and model predictions for all cases. It is however convenient to have some guidelines when selecting the decay factor, and several procedures have been presented in the literature. Some guidelines only focus on getting the best possible model predictions while others also focus on improving the conditioning of the least-squares problem. One possibility is to include α as an unknown parameter; thus, Eq. (12) becomes a nonlinear least-squares problem. The properties of Laguerre filters consisting of a low-pass and an all-pass filter have been well documented in the literature (Schetzen, 1980). These properties are also shown in Eqs. (8) and (9). In the control research community, authors (Campello et al., 2001, 2003, 2006; Fu and Dumont, 1993) have utilized pole placement of the filters in the z-domain to gain an optimal decay parameter by minimizing the model truncation error. Some authors have even suggested having different decay parameters for each filter and each order (Israelsen and Smith, 2014).

In this work, we choose a more straightforward form of the decay-parameter identification given in (Marmarelis, 1993). The reason for using the simple relationships given below is the ease of use, and sensitivity studies on experimental data show that the fit using this procedure gives a fit very close to the global minimum. The procedure is as follows:

1. Choosing a minimum decay parameter to obtain coefficients that are close to orthogonal:

Choose a decay parameter such that the cutoff frequency of the highest filter is less than the highest input frequency of the system:

$$\alpha \geq \left(2 - \cos(\beta) - \sqrt{\cos^2(\beta) - 4\cos(\beta) + 3}\right)^2 \tag{22}$$

where

$$\beta = 2\pi \frac{f_{\max}}{f_s} \tag{23}$$

where $f_{\max}$ is the maximum input frequency and f_s is the sampling frequency.

2. The highest filter used also has the longest influence (Marmarelis, 1993); suggested a heuristic relationship in which the IRF of the highest filter should be beneath a value cut for the end of the system memory to capture the entire memory and avoid overfitting.

$$g_J(M) \leq 0.01 \tag{24}$$

If the suggested decay parameter from Eq. (24) is lower than the minimum value of Eq. (22) one should decrease the number of filters. If the training data is white noise, ill-conditioning is not a problem, and Eq. (22) can be disregarded. A suitable model order and filter order can also be found by gradually increasing their values until the model performance stagnates when it is evaluated for an independent set of validation data.

3.3. The use of Volterra model full-scale time-domain calculations

To be able to use the Volterra models trained with experimental data on a full-scale analytical time-domain model, often using commercial FEM software, one needs to consider the following: 1) scaling from model scale to full scale, and 2) the possible resampling of the kernels.

1) Scaling

To be able to scale the mathematical model from model scale to full scale, the model is trained on dimensionless quantities that obey scaling laws. A commonly used scaling law in bridge aerodynamics is that an air particle uses the same dimensionless time to travel along the cross-section width at both the full and model scales. The dimensionless time *s* is given the following definition:

$$s = tV/B \tag{25}$$

where *V* is the mean wind speed and B is the deck width. The aerodynamic force can be made dimensionless by training the model with the equivalent static coefficients:

$$C_D = \frac{F_D}{\frac{1}{2}\rho D V^2},\ C_M = \frac{F_M}{\frac{1}{2}\rho B^2 V^2},\ C_L = \frac{F_L}{\frac{1}{2}\rho B V^2} \tag{26}$$

Table 1
Parameters of the theoretical example.

$d = V = B = 1$	$a_1 - a_5 = \{1, 0.05, 0.005, 0.0005, 0.00005\}$
Signal-to-noise ratio = 10[a]	$\alpha = 0.909$
Length of training data = 1.000.000	Length of validation data = 1.000.000
$J = 3$ $M = 100$	$dt = 0.05$sec

[a] Signal-to-noise ratio based on the variance of the signals.

where D is the cross-wind dimension (height) of the deck and ρ is the air density. The rotations are already dimensionless, and the displacement can be made dimensionless by dividing the motions by the bridge width B:

$$R_n = \frac{r_n}{B}, \quad where\ n = \{z, x\} \tag{27}$$

2) Resampling of kernels

The next point of discussion is the discrete nature of the Volterra kernels, which are obtained for a given intersample time. While this is not problematic in training, it can pose a problem/restraint on the time step in full-scale model simulations. Consider the following example:

Assume in a full-scale simulation of a suspension bridge excited by turbulent winds that the desired time step for integration is 0.2 s (corresponding to a 5 Hz sample rate and thus a 2.5 Hz Nyquist frequency). Furthermore, the wind velocity is 10 m/s in the wind tunnel and 50 m/s at full scale. The deck width B is set to 0.74 at the model scale and 37 m at the full scale, corresponding to a 1:50 geometric scale. The required intersample time for the model scale would then yield:

$$dt_{\mathrm{mod}} = dt_{full} \cdot \frac{V_{full}}{V_{mod}} \frac{B_{mod}}{B_{full}} = 0.2 \cdot \frac{50}{10} \frac{1}{50} = 0.02 \text{ s}$$

which corresponds to a sample rate of 50 Hz. The nondimensional time step is:

$$ds_{\mathrm{mod}} = ds_{full} = dt_{full} \cdot \frac{V_{full}}{B_{full}} \approx 0.27$$

It can be expected that the maximum nondimensional memory is approximately $s = 10$, implying that the effective length of the wake influencing the bridge is less than 10B (Costa and Borri, 2006; Øiseth et al., 2011; Wu and Kareem, 2014). The effective wake influence length requires a discrete memory of $M = 10/0.27 = 37$ time steps. Considering, for example, a 3rd-order Volterra series model, $M = 37$ can be very challenging for both identification and prediction, as it involves approximately 56,000 coefficients in the full nonparametric model. On the other hand, a Laguerre expansion basis using J = 7 filters only has 585 coefficients.

Furthermore, in the case of bridge simulations with nonlinear aerodynamics using FEM software, the time step is not necessarily directly coherent with the discretization of the Volterra kernels. The inconsistency requires resampling of the kernels. In this problem, it can be advocated that downsampling rather than upsampling is desired, which also imposes requirements for the minimum sampling rate of the wind tunnel data.

The memory size and speed in making the regression matrix in Eq. (10) are relevant for time-domain models. If one uses the recurrence relation of Eqs. (17) and (18), this effect is optimized. If the model has longer memory lengths than the filter order of the Laguerrian filter, as is often the case, the regression matrix size decreases significantly by using the Laguerrian expansion basis.

Note also that one should make use of the symmetry of the kernels when one implements the Volterra model.

4. Numerical example

A numerical example is created to evaluate the performance of the Laguerrian expansion based on relevant bridge aerodynamics. First, a linear kernel has been assumed to follow the impulse response function of a rational function (Øiseth et al., 2011), excluding the instantaneous terms:

$$h_1 = -\frac{dV}{B} e^{\left(-\frac{dV}{B}t\right)} \tag{28}$$

Next, static nonlinearity, in other words, a Weiner model, is introduced:

$$F = a_1 F_1 + a_2 {F_1}^2 + F_{noise} \tag{29}$$

where F_1 is the force from the convolution of the 1st-order kernel and the input. a_1 and a_2 are constants. A simulated white noise input is fed through the model, and the input-output data are used to train the Laguerrian expansion basis model, noise is added to the output. Three scenarios with different types of additional noise are studied:

1. SNR (signal-to-noise ratio) = ∞: Noise-free – Input-output data ($F_{noise} = 0$), i.e., no noise is added to the output, representing a perfect input-output data scenario.
2. SNR = 10: F_{noise} is artificial Gaussian white noise with an SNR (signal-to-noise ratio) equal to 10 (based on the variance of the signals), representing a scenario with imperfect measurements.
3. HO. Noise: Noise is added to the output by expanding the Weiner model with 3rd-, 4th- and 5th-order elements ($F_{noise} = a_3 {F_1}^3 + a_4 {F_1}^4 + a_5 {F_1}^5$), representing a scenario with a small number of high-order unaccounted dynamics. Note that the identification model is still limited to the 2nd order.

In Table 1, the general parameters of the numerical examples can be found. The decay factor α is found by using Eq. (24).

Fig. 5 shows the estimated kernels compared with the theoretical kernels. For scenarios 1 and 2, a very good fit with the theoretical kernel is obtained. In Fig. 5b), it can be seen that the higher-order noise (scenario 3) has a slight influence on the diagonal of the 2nd-order kernel, which is probably because the inclusion of the 4th-order noise is also a one-sided nonlinearity. Similar effects can be observed for the 1st-order kernel, where the 3rd- and 5th-order dynamics embed as an erroneous kernel contribution. However, the kernels still look similar in shape and form, and the identified kernels have the correct decay. The example shows that the Laguerrian expansion basis (LEB) is efficient for low-order models that are used for predicting nonlinear self-excited forces.

In this work the quality of fit in the time-domain is generally checked with the normalized mean square error (NMSE):

$$\mathrm{NMSE} = 1 - \frac{\left\|\mathbf{x}_{ref} - \mathbf{x}_{pred}\right\|^2}{\left\|\mathbf{x}_{ref} - \mathrm{mean}\left(\mathbf{x}_{ref}\right)\right\|^2} \tag{30}$$

where $\mathbf{x}$ is the predicted data and $\mathbf{x}_{ref}$ is the measured data. $\|\mathbf{x}\|$ represents the second norm of the vector $\mathbf{x}$. The NMSE value is 1 for perfect fit and -∞ for a very poor fit.

Fig. 6 shows a time-domain realization of the different models, where new white noise inputs are used to validate the realizations. All three models fit very well. Note that the NMSE values are very high for all models, where the scenario with higher-order dynamics yields a slightly lower value of 0.962.

As mentioned in Chapter 3.1, the Laguerre IRFs are orthonormal. This property implies that the coefficients are uncorrelated with each other, given that the input is Gaussian white noise. Thus, increasing the filter order by one in the identification problem does not influence the coefficients of the lower-order filters. This property is confirmed for the

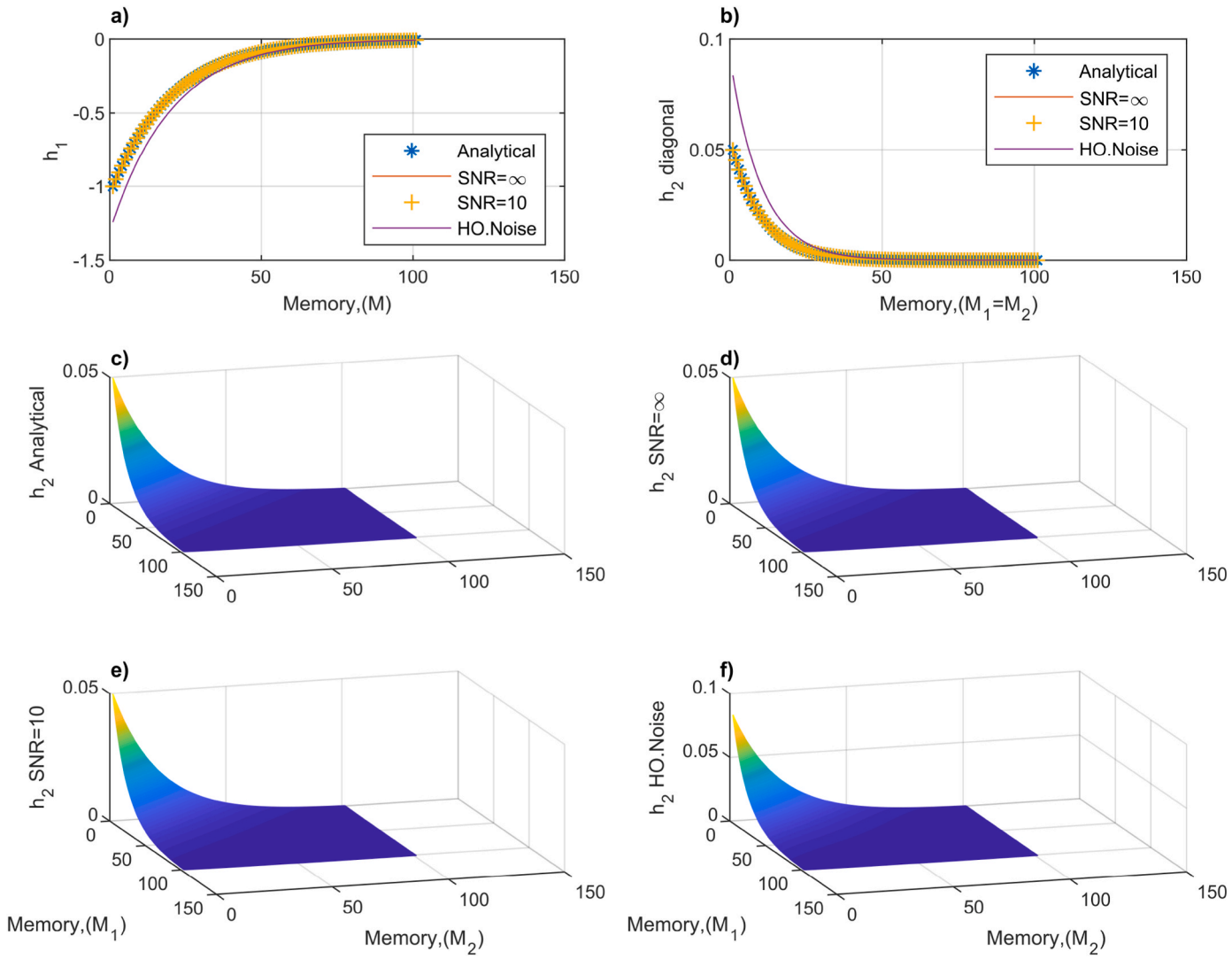

Fig. 5. Theoretical example of LEB training. a) 1st-order kernel, b) diagonal of 2nd-order kernel, c) 2nd-order kernel analytical, d) 2nd-order kernel for input-output data without noise, e) 2nd-order kernel with added white noise in the output, f) 2nd kernel trained for input-output data with added higher-order component.

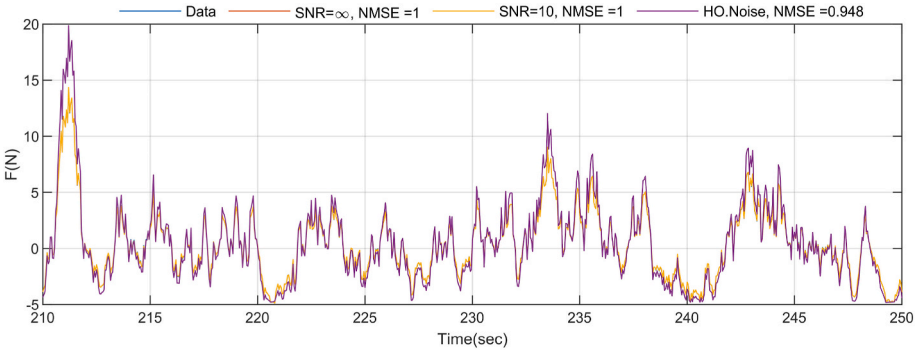

Fig. 6. Time-domain realization of the different trained Volterra models.

numerical example in Table 2, which shows the resulting coefficients from Eq. (13) for filter orders $J = 1$, $J = 2$ and $J = 3$. The table also shows that setting the memory as $M = 30$ and $M = 100$ yields the same results, as the recursive relationship of Eq. (17) is used.

If the same system is excited with pink noise, slightly different coefficients are obtained between the 1st and 2nd filter orders. Another interesting fact from the table is that when using a filter order of two or higher, the coefficients become almost similar independent of the input. This concurs with (Marmarelis, 1993), who stated that orthogonality effects are also achieved for colored noise input as long as a sufficiently high model and filter order are used.

Table 2
Estimated coefficients for different filter orders, with different memory lengths and with and without constant terms. Note that all models have been trained with the recursive relation of the regression matrix. The model order is P = 2.

	$M = 30$			$M = 100$			$M = 100$		
Input data:	white noise			white noise			pink noise		
Regression column, x	$J = 1$	$J = 2$	$J = 3$	$J = 1$	$J = 2$	$J = 3$	$J = 1$	$J = 2$	$J = 3$
1	0.0000	0.0000	0.0000	0.0000	0.0000	0.0000	0.0005	0.0000	0.0000
x1	−3.2409	−3.2408	−3.2408	−3.2409	−3.2408	−3.2408	−3.1877	−3.2406	−3.2406
x2	–	−0.0762	−0.0762	–	−0.0762	−0.0762	–	−0.0757	−0.0758
x1x1	0.5250	0.5251	0.5251	0.5250	0.5251	0.5251	0.5084	0.5250	0.5250
x1x2	–	−0.0247	−0.0247	–	−0.0247	−0.0247	–	−0.0246	−0.0245
x2x1	–	Sym.	Sym.	–	Sym.	Sym.	–	Sym.	Sym.
x2x2	–	0.0003	0.0003	–	0.0003	0.0003	–	0.0003	0.0003
x3	–	–	−0.0015	–	–	−0.0015	–	–	0.0000
x1x3	–	–	0.0005	–	–	0.0005	–	–	0.0003
x2x3	–	–	0.0000	–	–	0.0000	–	–	0.0000
x3x1	–	–	Sym.	–	–	Sym.	–	–	Sym.
x3x2	–	–	Sym.	–	–	Sym.	–	–	Sym.
x3x3	–	–	0.0000	–	–	0.0000	–	–	0.0001

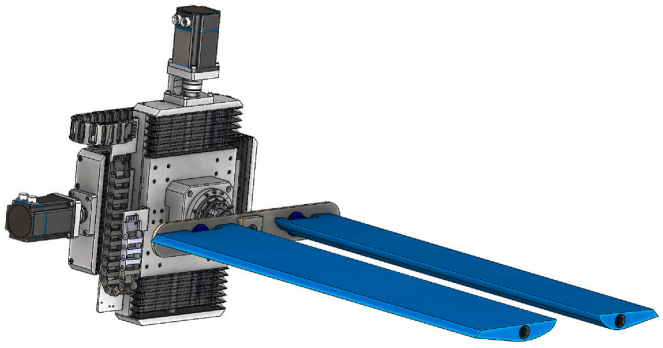

Fig. 7. Illustration of the forced vibration rig with the tested model mounted in the model.

Table 3
NMSE between experimental data and estimated model data from the Volterra series model of different orders using the Laguerrian expansion basis. 1DOF random pitching motion data. The models are compared to the performance of a linear benchmark model using a rational function approximation fitted to aerodynamic derivatives.

Section force	Mean wind speed	Rational function	1st	2nd	3rd	4th
Moment	10	0.893	0.905	0.981	0.983	0.983
Moment	6	0.919	0.983	0.989	0.992	0.992
Lift	10	0.959	0.978	0.993	0.994	0.994
Lift	6	0.984	0.989	0.992	0.995	0.995
Drag	10	−0.124	0.642	0.938	0.942	0.942
Drag	6	0.117	0.391	0.882	0.905	0.905

5. Experimental example

A wind tunnel testing campaign was conducted at the Fluid Mechanics Laboratory at the Norwegian University of Science and Technology (NTNU). A 1:50 twin deck section model with curved undersides was tested. The cross-section exhibits slightly nonlinear properties in the self-excited pitching moment and severe nonlinearities in the self-exited drag for tests with low amplitudes. For a more detailed description of the campaign, see (Skyvulstad et al., 2021). The wind tunnel facility has an advanced forced vibration rig driven by motion actuators that can excite the cross-section in an arbitrarily prescribed vertical, horizontal and pitching motion. The rig is fully described in (Siedziako et al., 2017). Fig. 7 shows an illustration of the section model in the rig. Drag, lift and pitching moment forces are measured by load cells at each end of the section model at a sampling frequency of 250 Hz.

A variety of tests were performed on the section model, including single harmonic motion and random motion tests. Random motion tests are well suited to excite a wide frequency range in a short amount of time and are the preferred choice for system identification of a general load model. The largest amplitudes of the tested pitching motion are about 2.5°, which implies that significant nonlinearities are only expected for the drag force. However, all sections have nonlinear aerodynamic behavior for large angles of attack, which can be caused by large motion or large-scale incoming turbulence that contributes to the dynamic angle of attack.

The inertia forces are removed from the analysis by utilizing the (Han et al., 2014) method, which implies testing the same motion in still air and subtracting the forces from the forces in the in-wind test. The contribution from self-excited forces in still air is assumed to be insignificant.

The goal of the rest of this chapter is to evaluate the performance of the Laguerrian filter basis technique on nonlinear self-excited forces for bridge decks with low amplitude motions. Nonlinear forces for low amplitude motions are interesting. Usually, nonlinearities are seen for damping-driven high amplitude motion phenomena such as galloping, vortex-induced vibrations, and torsional flutter. However, the nonlinear behavior for small amplitudes is interesting for a broader range of bridge responses and for the ultimate limit state response in turbulent winds.

In the next chapter, 1DOF random pitching motion experiments are used to evaluate the Laguerrian expansion basis technique. Furthermore, the most nonlinear component, namely, the 6 m/s self-excited drag force, is evaluated in detail. After that, 2DOF random motion tests are evaluated, and the 6 m/s drag force is investigated in detail.

5.1. One degree of freedom random pitching motion

In the following, the 1st^{-} to 4th-order Volterra models with different filter orders (J = 1-10) are calibrated and validated on experimental data utilizing the Laguerrian expansion basis. The motion in the wind tunnel is a time-domain realization of colored noise with a constant spectrum between 0 and 3.5 Hz, which corresponds to a full-scale frequency content (V = 50 m/s) of 0–0.31 Hz. Three hundred seconds of training data and 300 s of validation data are used. The wind speed in the tunnel is 6 and 10 m/s, and the motion forced on the cross-section is pitching motion. The wind tunnel test is sampled at 200 Hz but is downsampled by a factor of 1/3 (~66.6 Hz), and the downsampling is in agreement with the sampling rate applicable for utilizing the model at full scale. The amplitude of the model is restricted to a maximum amplitude over the entire time series of 3°.

For each Volterra model order, the lowest filter order that gave the

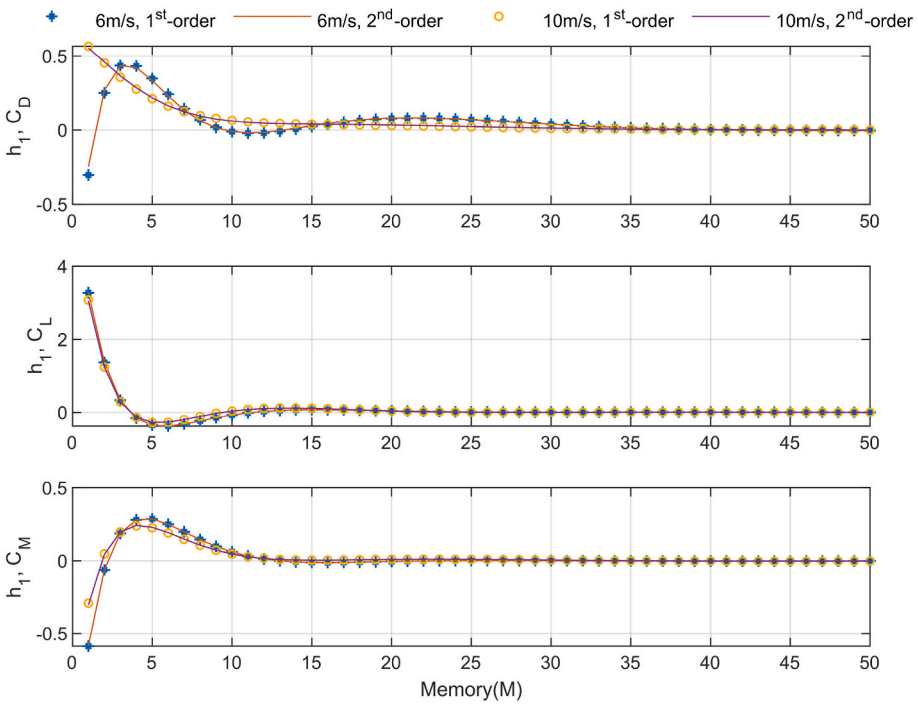

Fig. 8. 1st-order kernel of different models. Self-excited pitching-motion data are used for calibration of the model. Note that the 1st-order kernel of the 1st-order models can be viewed as the linear unit impulse response function of the system.

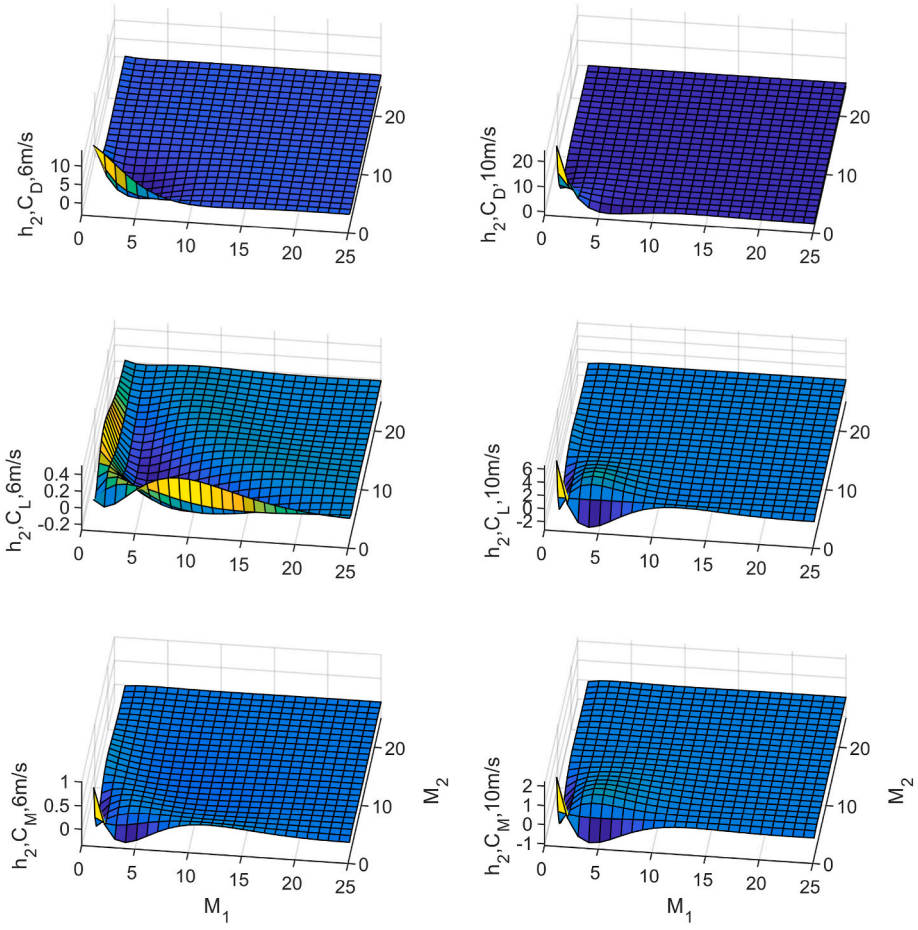

Fig. 9. 2nd-order kernels for different models. Self-excited random pitching motion.

Table 4
Comparison of different orders of the Volterra series model performance according to NMSE. The models are compared to the performance of a linear benchmark model using a rational function approximation fitted to aerodynamic derivatives.

	Rational function	1st	2nd	3rd	4th
NMSE	0.117	0.39	0.88	0.905	0.905

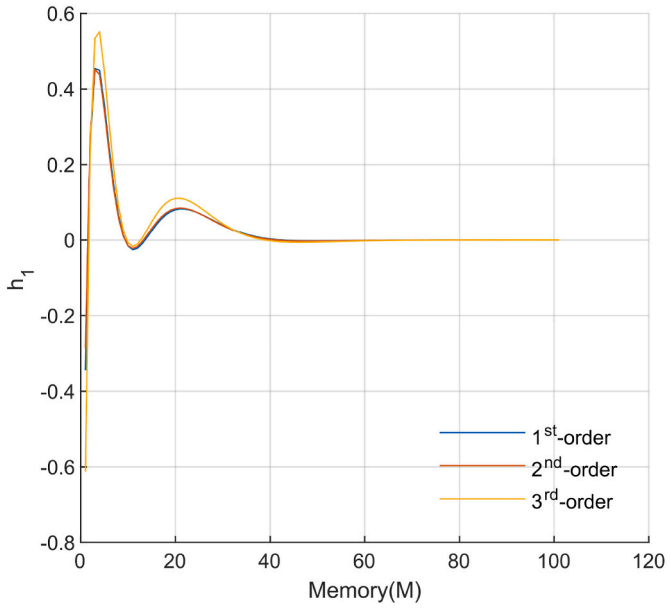

Fig. 10. 1st-order kernels for the 1st^{-}, 2nd^{-} and 3rd-order models. Drag force at 6 m/s for pitching motion training data. Note that the higher-order models include all lower-order kernels. As an example, the 3rd-order model has 1st^{-},2nd-order and 3rd-order kernels.

best performance according to the NMSE was chosen. Filter-order $J = 5$ gives the best fit for all orders of the model, and utilizing the heuristic relation of Eq. (24) gives an $\alpha = 0.6563$. A sensitivity study to change α finds that the fit is relatively independent of the factor.

The NMSE values are given in Table 3. It can be seen in the table that the drag force measured at 6 m/s wind speed is the most nonlinear force component since the NMSE is only 0.391 for the 1st-order model. These tests are evaluated in detail in the next chapter. This section mainly focuses on other results. It is seen in the table that the lift and the 6 m/s pitching moment are more or less linear with an NMSE above 0.98. The 2nd-order model increases the performance for the 10 m/s pitching moment and 10 m/s drag. 3rd-order models provide only a slight increase in all model performances. The 4th-order model gave no extra gain in performance but did not suffer from overfitting either.

The performance of a rational function model (Øiseth et al., 2011) is presented in Table 3 to evaluate the Laguerrian expansion basis models performance against a well-established model in bridge aerodynamics. The rational function model is established from a fit to the aerodynamic derivatives, which is in turn is extracted from single harmonic tests (Skyvulstad et al., 2021). Since the cross-section is found to be Reynolds-sensitive, only single harmonic data, with the same mean wind speed as the validation data, were used to extract the aerodynamic derivatives.

It is seen from the table that the 1st-order Volterra-models perform better than the rational function models. A reason for this could be that more terms have been used in the Laguerrian expansion basis than in the rational function approximation. Another reason is the greater similarity of training and validation data used for the Laguerrian expansion basis. Nevertheless, this illustrates that the Laguerrian expansion basis also has potential for linear modelling of self-excited forces.

Fig. 8 shows the 1st-order kernels for the different force components for motion tests at different wind speeds. It is interesting to note that the change in mean wind speed drastically changes the 1st-order kernel in drag, but the kernels for lift and pitching moment remain the same. This change could be explained by a Reynolds number dependency of the cross-section. The 1st-order kernel for the lift and pitching moment shows only small differences in the different mean wind speeds, indicating less Reynolds number dependency for these sectional forces. The 6 m/s pitching moment kernel has a larger negative starting value than the 10 m/s kernel, but it also has higher positive values evening out the differences.

Fig. 9 shows the 2nd-order kernels for different models. As expected, the parameterized kernels yield surfaces that are generally smooth. The 2nd-order kernels for drag are also different for both wind speeds, but the shape is not as different as seen for the 1st-order kernel. The lift kernel shapes are also different, but note that the 6 m/s lift kernel is numerically very small, indicating less nonlinearity of the time series, as also seen in Table 3. The difference in absolute values of the 2nd-order kernel for the 6 m/s and 10 m/s tests is quite significant, and the larger numerical values of the 10 m/s kernel indicate that the system is more nonlinear than the 6 m/s test, which is also seen in Table 3. For the 2nd-order kernel, the memory lengths are approximately 10 elements giving a total 2nd-order memory length of $s_{2st,Memory} = 10*0.1216 \approx 1.2$. The exception to memory lengths is the 6 m/s lift kernel, but this kernel is almost zero and should not be included in the modeling of the lift force.

5.2. Drag force from one degree of freedom pitching motion

In this chapter, the 6 m/s self-excited drag force is investigated in detail. Table 4 shows a comparison between the different nonlinear model orders and their performance. Several comments can be made from the table: The 1st-order model struggles to predict the drag data, a clear indicator of nonlinearity. The 2nd-order model performs significantly better than the linear model, and the 3rd-order model performs slightly better than the 2nd-order model. The 4th-order model does not increase in performance compared to the 3rd-order model. Since the 4th-order model did not give a better prediction, this model was not investigated further.

Fig. 10 shows the 1st-order kernel for the 1st^{-}, 2nd^{-} and 3rd-order models. Note that the 1st-order kernel for the 1st-order model is the only kernel that can be said to be a linear impulse response of the system. The diagonal elements on the higher-order kernels can also be seen as "autokernels", and therefore, the 1st-order impulse response needs to account for the higher-order effects. In other words, the 1st-order kernel does not need to be the same for all of the models, which further implies that one cannot reduce a higher-order model to a lower-order model by removing the higher-order kernels. It is interesting to note that in the 3rd-order models, the 1st-order kernel has higher positive values on both peaks compared with the 1st^{-} and 2nd-order models. It seems that the extraction of 3rd-order nonlinearities enables the inclusion of more information in the linear kernel since both are odd order. The sharp edge of the kernel comes from the discrete form properties of the LEB, but the kernels are in general very smooth considering the noise level in the measurements, and this can be assigned to the low-pass filter properties of the Laguerrian filters. Volterra identification methods based on full nonparametric least-squares often yield nonsmooth kernels, making the physical reasoning behind the kernels more challenging to interpret.

The 1st-order kernel diminishes to zero at approximately 45 elements for all models. This means that the 1st-order memory of the system, in nondimensional time, is approximately $s_{1st,\ Memory} = 45*0.1216 \approx 5.5$. This corresponds to a physical length of 5.5*B, a result that can be reasonable for bridge decks.

Fig. 11 shows the 2nd-order kernels for the 2nd^{-} and 3rd-order models. The numerical value of the 2nd-order kernel is significant compared with the 1st-order kernel, which further implies that the 2nd-

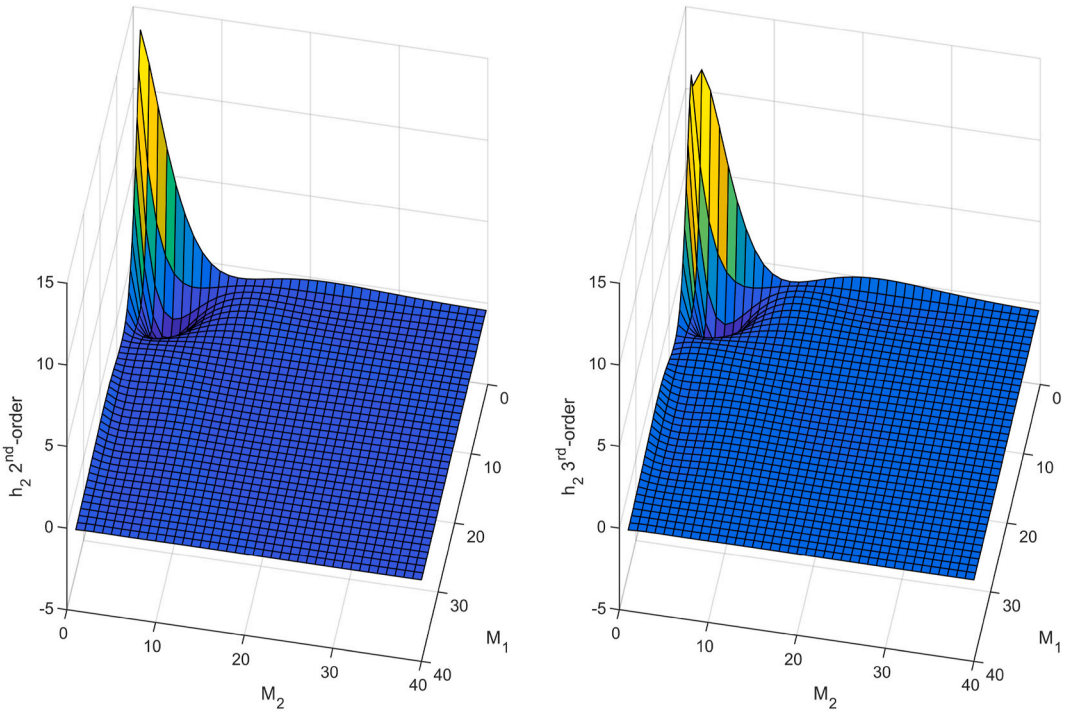

Fig. 11. 2nd-order kernels for the 2nd$^-$ and 3rd-order Volterra models. Note that the higher-order models include all lower-order kernels. As an example, the 3rd-order model has 1st$^-$, 2nd$^-$ and 3rd-order kernels.

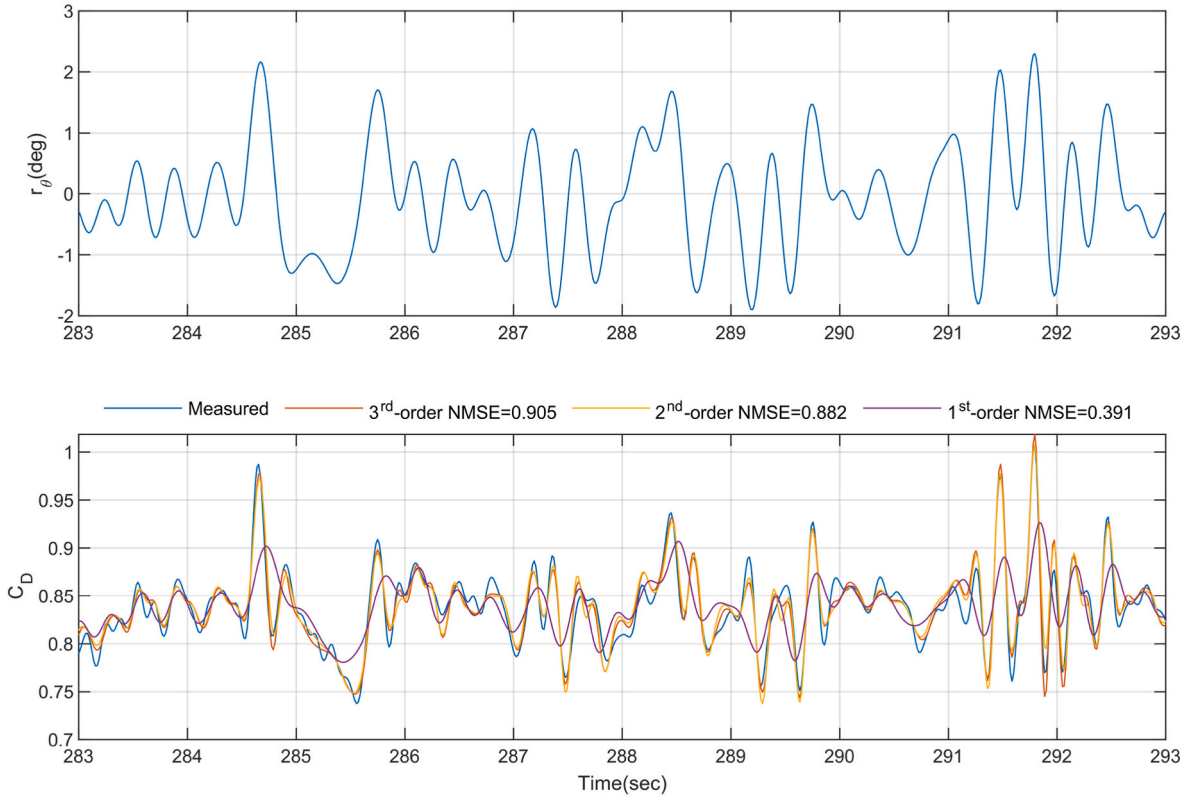

Fig. 12. Prediction of motion-induced forces using Volterra models of different orders compared to experimental data. Drag force 6 m/s random pitching motion data. Training data are independent of the validation data viewed.

order kernel is essential, as expected from the increased performance of the 2nd-order model compared with the 1st-order model. Note that the force output is dependent on the pitching motion in radians squared, so the magnitude difference cannot be compared directly.

The kernel shape is very smooth and has high similarities to the square of the 1st-order kernel. The experimental noise is very much

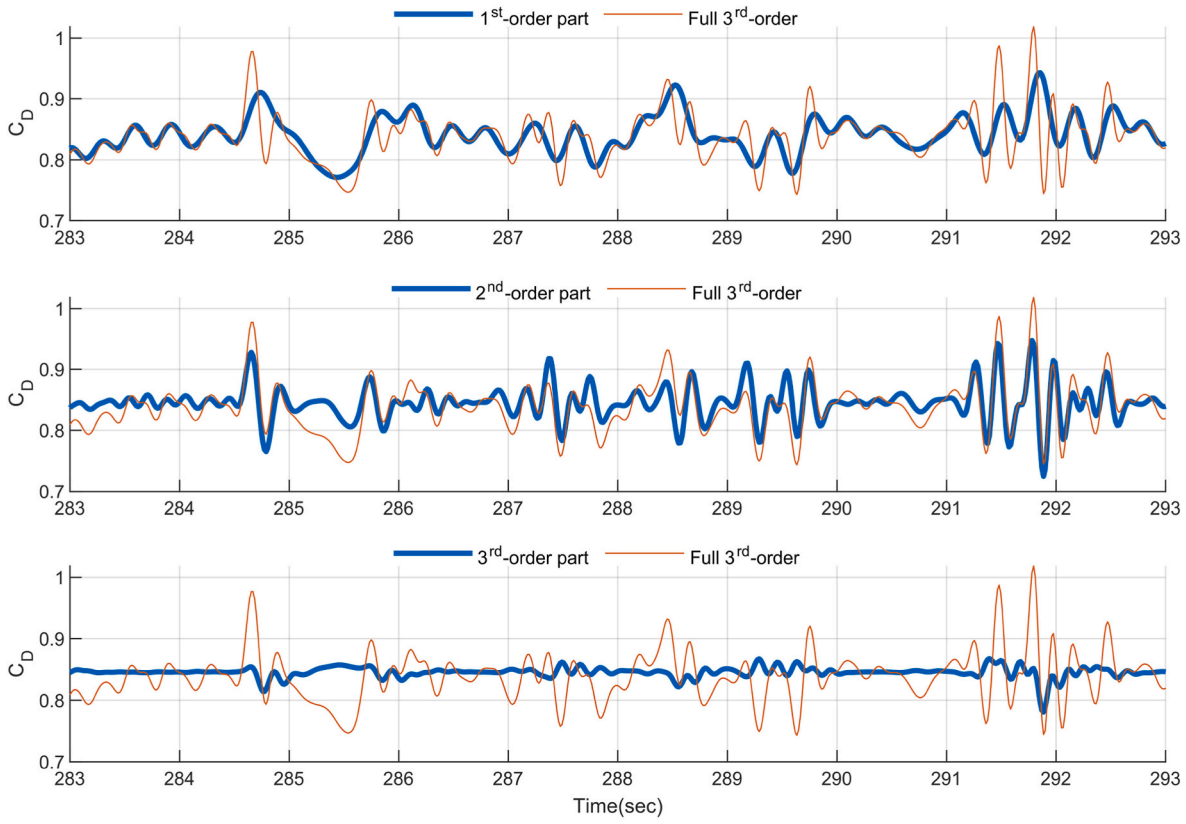

Fig. 13. Predicted self-excited drag force due to random pitching motion at 6 m/s wind velocity. The thick line in the top figure shows the contribution from the first 1st-order kernel, the thick line in the middle figure shows the contributions from the 2nd^{-} order kernel and the thick line in the bottom figure shows the contribution from the 3rd-order kernel. The thin lines show the sum of all contributions.

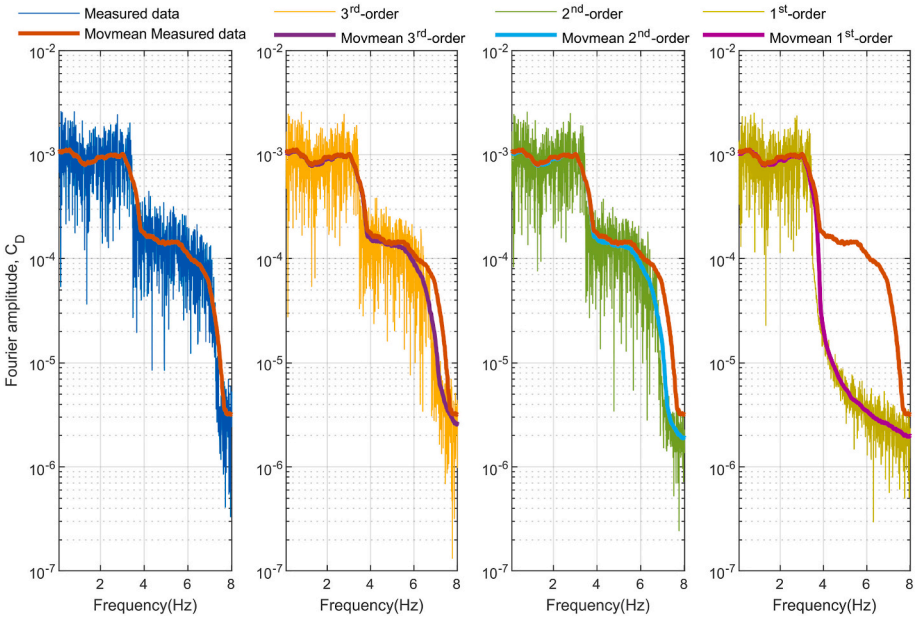

Fig. 14. Fourier amplitude of the predicted and the validation self-excited drag force data. Movmean denotes the smoothed 100-element central moving mean of the Fourier amplitude.

suppressed in the kernel, and the 2nd-order memory is significantly shorter than the 1st-order memory, at approximately 25 elements or a nondimensional memory $s_{2nd,\ memory} = 25*0.1216 = 3.04$. A reduction in higher-order memory lengths is expected, and this was utilized by (Wu and Kareem, 2014) by reducing the effective memory of the higher-order kernels. Some discrepancies of the 2nd-order kernel from the 2nd^{-} and 3rd-order models are visible, but these discrepancies can be characterized as small.

Fig. 12 shows a cut of the experiment's validation time series plotted together with the predicted time series from different model orders. The

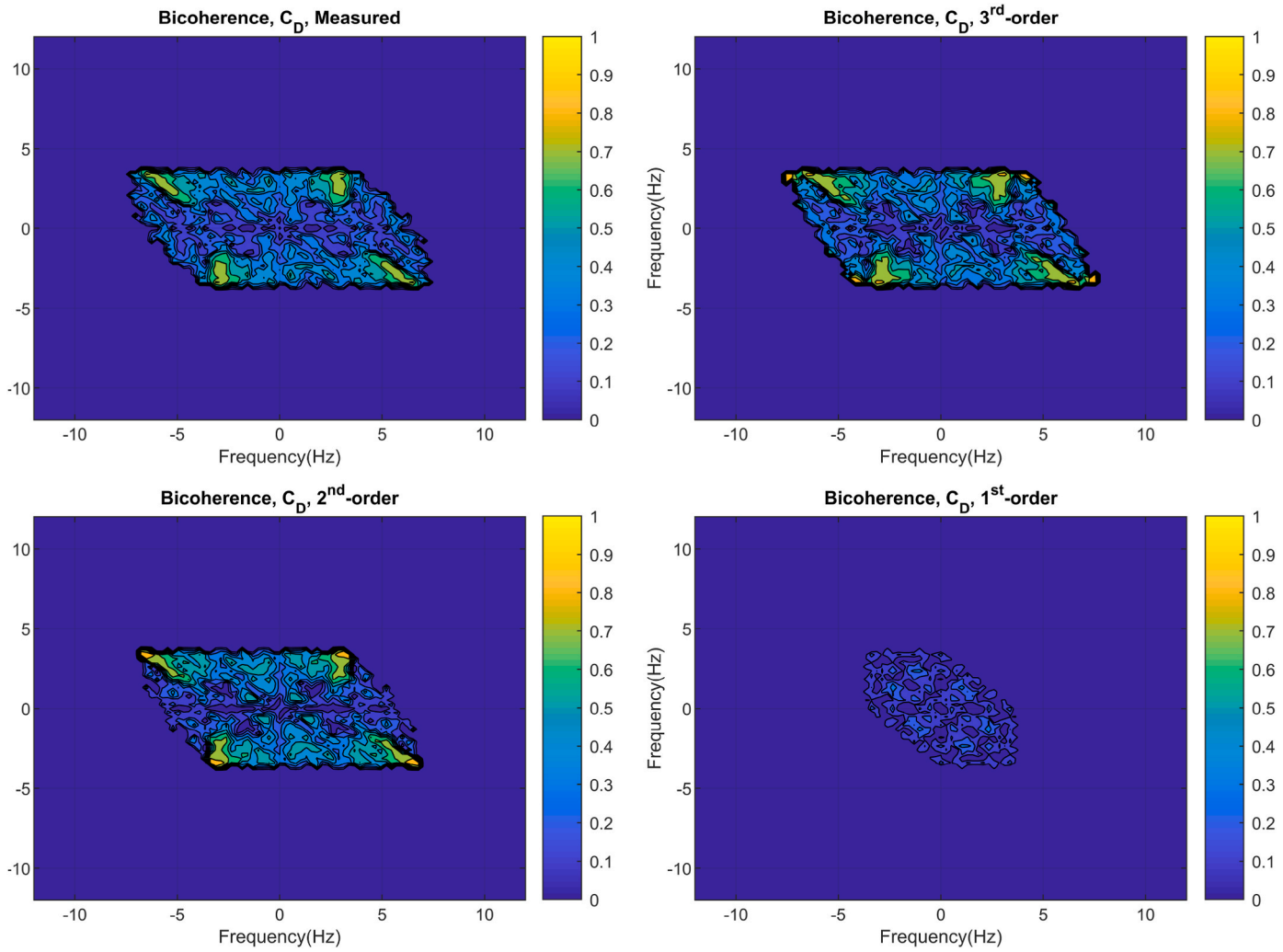

Fig. 15. Bicoherence values between the pitching motion, and the force from the measured validation data as well as the predicted force for the Volterra models at different orders. The data is the self-excited drag force at 6 m/s.

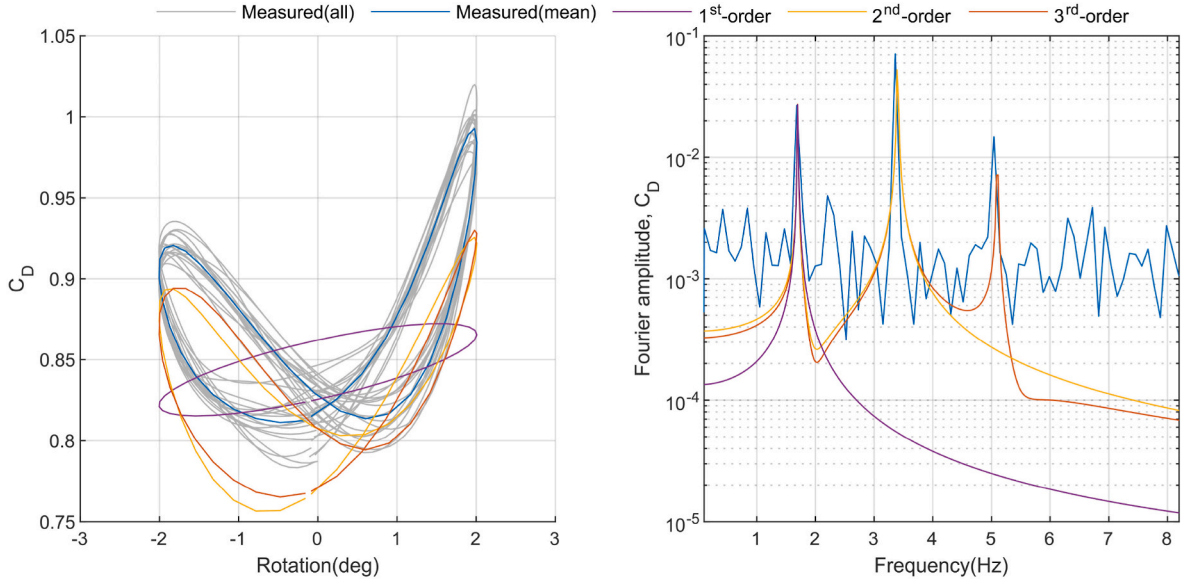

Fig. 16. Single harmonic experimental data, 6 m/s 1.7 Hz test pitching motion and Volterra model prediction from models calibrated on random motion 6 m/s pitching motion data. The power spectrum shows that the higher-order models are needed for modelling higher-order harmonics of the measured force.

Table 5
NMSE between experimental data and estimated model data from the Volterra series model of different orders using the Laguerrian expansion basis. 2DOF random motion vertical and pitching motion data. The models are compared to the performance of a linear benchmark model using a rational function approximation fitted to aerodynamic derivatives.

Section force	Mean wind speed	Cross	Rational function	1st	2nd	3rd	4th
Moment	10	Yes	0.854	0.903	0.977	0.975	0.970
Moment	10	No	0.854	0.903	0.947	0.945	0.945
Moment	6	Yes	0.937	0.979	0.985	0.988	0.976
Moment	6	No	0.937	0.979	0.982	0.982	0.980
Lift	10	Yes	0.941	0.961	0.976	0.971	0.939
Lift	10	No	0.941	0.961	0.970	0.969	0.967
Lift	6	Yes	0.951	0.965	0.968	0.967	0.924
Lift	6	No	0.951	0.965	0.967	0.967	0.964
Drag	10	Yes	0.187	0.612	0.770	0.735	0.394
Drag	10	No	0.187	0.612	0.726	0.701	0.670
Drag	6	Yes	0.408	0.503	0.815	0.821	0.755
Drag	6	No	0.408	0.503	0.724	0.725	0.719

Table 6
NMSE between experimental 2DOF random motion vertical and pitching motion data and superposition of 1 + 1 random motion vertical and torsional data.

Section force	Mean wind speed	1+1Dof
Moment	10	0.903
Moment	6	0.966
Lift	10	0.966
Lift	6	0.977
Drag	10	0.722
Drag	6	0.463

Table 7
Shows the NMSE performance of the different models. Volterra w/cross is a Volterra model using a Laguerrian filter basis but with cross kernels included. Volterra w/o cross is a Volterra model using a Laguerrian filter basis but without using cross kernels but calibrated with 2DOF data directly. Experimental denotes the superposition of the two 1 + 1 degree of freedom tests. The models are compared to the performance of a linear benchmark model using a rational function approximation fitted to aerodynamic derivatives.

Volterra w/cross	1st = 0.503	2nd = 0.815	3rd = 0.821	4th = 0.755
Volterra w/o cross	1st = 0.503	2nd = 0.724	3rd = 0.725	4th = 0.719
Experimental	1+1DOF = 0.463		Rational function	= 0.408

top of the figure shows the pitching motions. One can see in the figure that the 1st-order model struggles to predict the drag force. The amplitudes of the predicted force for the 1st-order model amplitude are always smaller than the measured ones, and the error becomes greater with higher amplitude motion. The results are expected if high 2nd-order nonlinearity is present, as often is the case for drag.

The 2nd^{-} and 3rd-order models perform significantly better than the 1st-order model. It is interesting to note that the 2nd^{-} and 3rd-order models follow each other very closely and that the 3rd-order model only slightly alters behavior compared with the 2nd-order model. A surprising fact is that the high amplitude forces are also predicted as the low amplitude forces, and it seems that more discrepancies are present for low-amplitude high-frequency motions of approximately 286 s–287.5 s. The discrepancies could be due to the suppression of higher-order noise by the filters, or it could be a 4th^{-} or higher-order nonlinearity present system.

Fig. 13 shows a breakdown of the 3rd-order model prediction. It is seen that the 1st-order part has lower frequency components compared with the 2nd- and the 3rd- order contribution. It is interesting to note

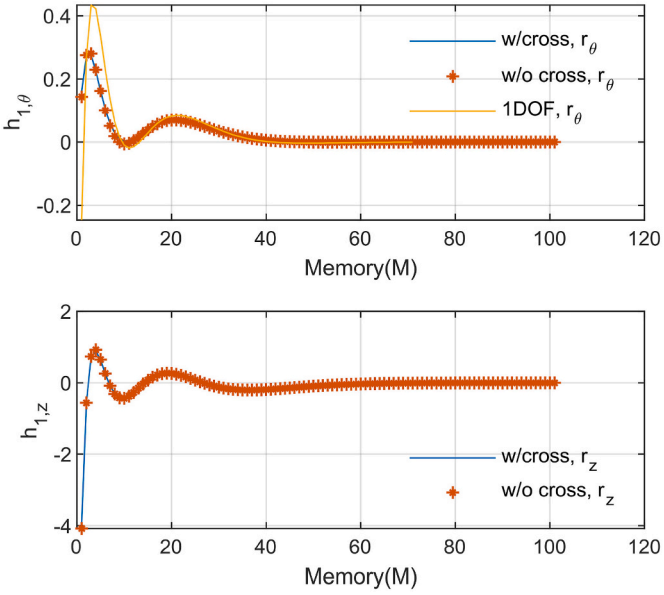

Fig. 17. 1st-order kernel for both inputs of the cross model. 6 m/s random motion, drag data with vertical motion and pitching motion as input. Kernels are from 2nd-order models.

that the 3rd-order contribution contributes mostly when the pitching motion is large.

Fig. 14 shows the Fourier amplitudes for the different Volterra-models compared with the Fourier amplitude of the validation data for the self-excited drag force. Moving mean values are also shown. The figure shows that the 1st-order model lacks frequency content above the highest input frequency of 3.5Hz. The 2nd-order model captures the high-frequency components and the 3rd-order model is the most accurate of the considered models.

Bicoherence is a tool that can be used for identifying the quadratic coupling of frequencies in a signal. Fig. 15 shows the bicoherence between the motion input and the self-excited drag force for the validation data and the predicted forces. The predictions from the 1st, 2nd, and 3rd-order models, where bicoherence definition used is according to (Hayashi et al., 2007). The bicoherence is always between zero and one, respectively representing the case of no quadratic coupling and the case where all energy stems from a quadratic coupling for that frequency pair. It is seen from Fig. 16 that the measured data has a strong quadratic coupling for values outside the input region of 0–3.5 Hz, but the quadratic coupling is also present within the frequency range of the input motion. For the linear model, on the other hand, very low values of the bicoherence are observed as expected since no quadratic nonlinearity is present in this model. The 3rd-order and the 2nd-order model both show a very similar pattern of bicoherence as the measured validation data. Using the bicoherence tool one can observe that the 2nd^{-} and 3rd-order model has very similar quadratic frequency content compared with the measured validation data.

When the model is trained on the random motion data, one can predict forces on any arbitrary motion. Of course, one should be very careful to predict forces from motions that are outside the training region of the model, considering amplitude, frequency, and motion history over the memory length. Fig. 16 shows a 1.7 Hz single harmonic test at 6 m/s compared with predicted forces from the Volterra models trained on random motion data. The amplitude of the single harmonic is 2°, and the frequency is 1.7 Hz, which is inside the testing region data of the random motion, so one should expect reasonable behavior from the Volterra models. Note that testing of a single harmonic represents a very distinct motion pattern backwards in time and that the single harmonics (14 cycles) are shown, but the first two cycles are removed to stabilize the fluid memory over the cycles. The stabilized motions are probably

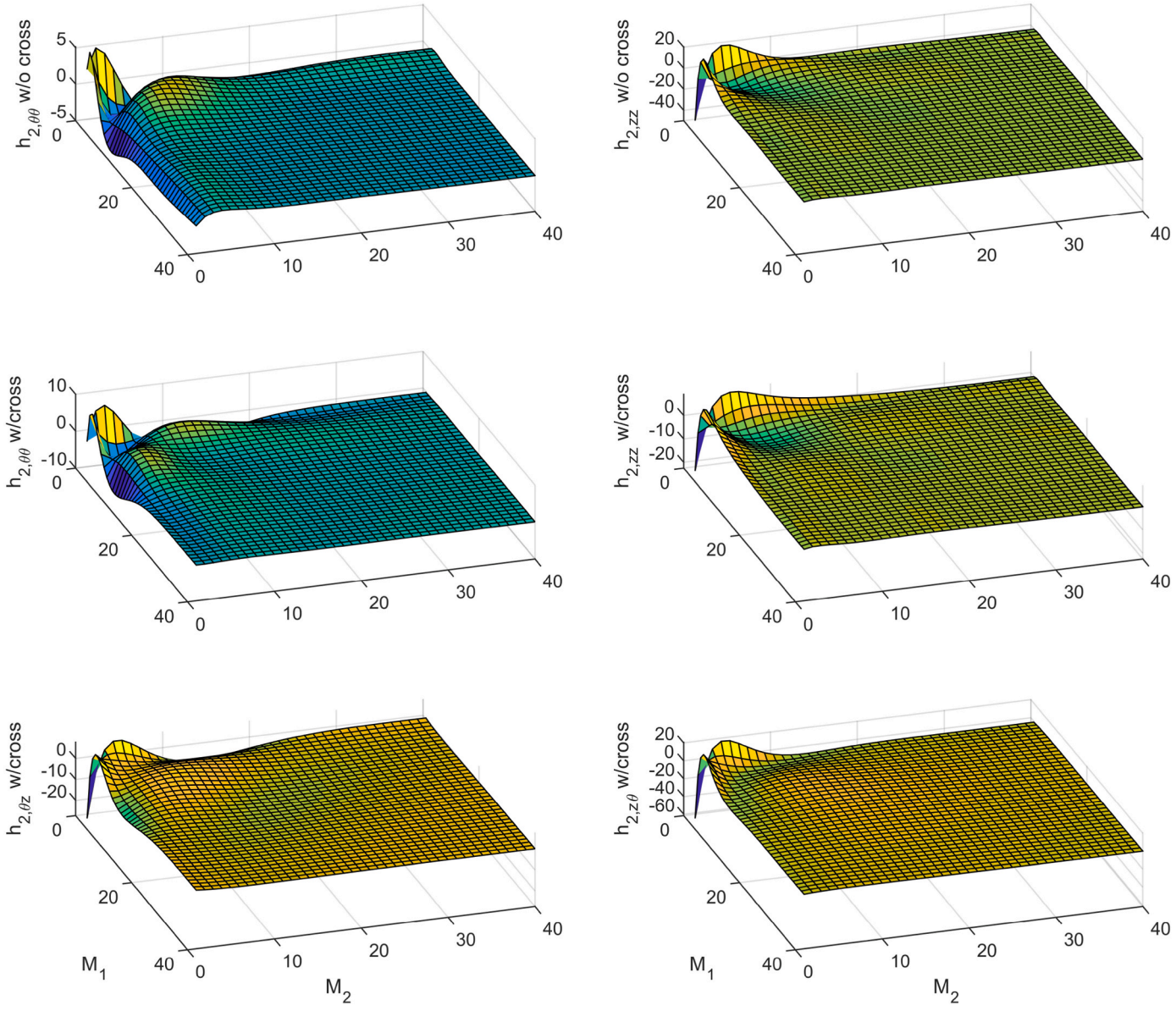

Fig. 18. 2nd direct and cross kernels for the 2nd-order Volterra model. 6 m/s drag force data with pitching motion and vertical motion as input. Note that input 1 is pitching motion, and input 2 is vertical motion.

outside the testing region of the random motion.

The 1st-order model shows typical linear elliptical shapes in the hysteresis plot. This is limited to predicting only the 1st-order harmonic, as seen in Fig. 16. The 2nd^{-} and 3rd-order models can predict 2nd and 3rd superharmonics as expected, but it can be seen that the 3rd-order model somewhat underestimates the 3rd superharmonic.

The performance of the hysteresis predicted by the 2nd^{-} and 3rd-order models is acceptable but not very impressive. Note also that significant mean drift effects between predicted and measured tests are present. The Volterra model can model mean drift effects, but as expected, using stochastic training data when predicting the forces from single harmonics will deem some inaccuracies.

5.3. Two degrees of freedom pitching and vertical motion

Two degrees of freedom random motion is also tested in the wind tunnel. Herein, the two degrees of freedom data comprise vertical and pitching motions. The pitching motion is the same as for the 1DOF motion in the previous chapter. The vertical motion is also a time realization of colored noise with a constant spectrum between 0 and 3.5 Hz. The maximum amplitude of the vertical motion is 30 mm.

Note that all models are based on the displacements as input. Vertical velocity is directly related to the change in the angle of attack according to quasi-steady theory, but analysis has shown that using displacement as input gives the same results. It is important to note that the displacement is not an independent variable compared with the velocity, and models with memory will also be velocity dependent for displacement inputs.

A 1DOF vertical motion with the same vertical motion amplitudes of the 2DOF motion is also tested in the wind tunnel, providing an opportunity for a benchmark of superposition experimental tests.

Table 5 and Table 6 show the NMSE performance of the different models for 2DOF random motion data. The Laguerrian filter basis is iterated from filter order J = 0-10 with the decay factor determined by the highest filter according to Eq. (24). All models used a filter order of J = 5 and a decay factor of $\alpha = 0.6563$.

Table 5 shows the NMSE performance on the 2DOF self-excited force data. Including cross-terms gives, in general, an increase in performance

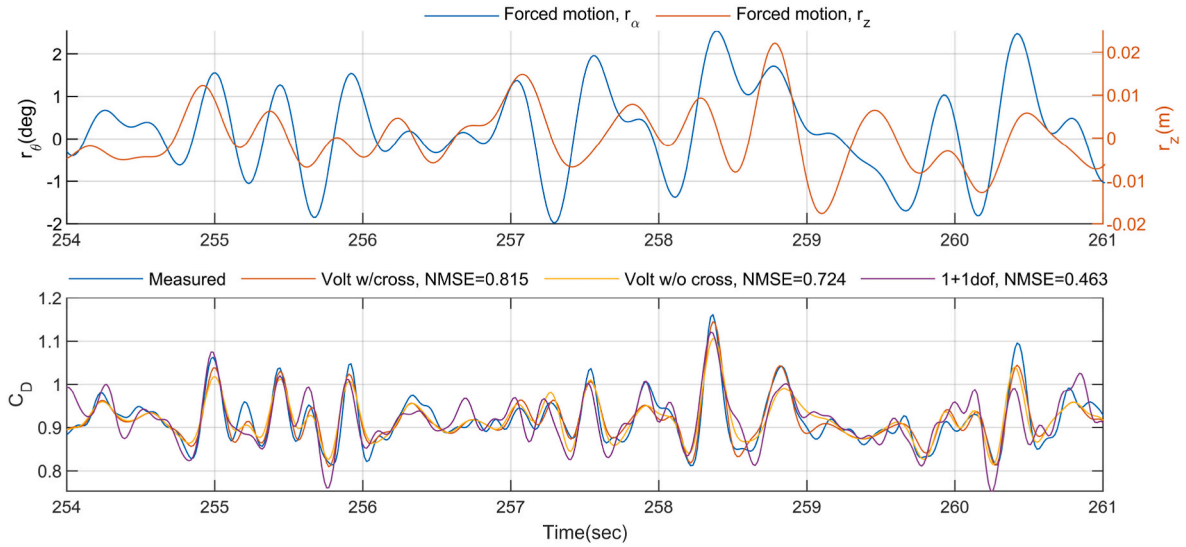

Fig. 19. Time-domain realization of different Volterra series models compared with experimental data. Volt w/cross denotes full 2nd-order Volterra with cross-terms. Volt w/o cross denotes the 2nd-order Volterra model without cross-terms. 1+1DOF denotes the superposition of a single degree of experimental data. 6 m/s drag force data.

for all 2nd$^-$ and 3rd-order models. The performance decrease of the 4th-order model shows clear signs of overfitting, but the performance loss is generally small.

The performance of the Laguerrian expansion basis for modeling 2DOF lift and pitching moment data is good, but modeling the drag force is challenging, and the 6 m/s drag data for 2DOF motions are evaluated in detail in the next chapter.

The Rational function model benchmark of the 1DOF case is also introduced in the 2DOF case. It is seen that the 1st-order Volterra models outperform the rational function model. The reason for this could be assigned to the type of rational function model, but the reason is probably due to the difference in training data compared with the validation data. Nevertheless, this indicates that the Laguerrian expansion basis models perform well on the problem at hand.

Table 6 shows the performance of the superposition of two 1DOF motions, namely, vertical and pitching motions. The performance should be compared with the models given in Table 5.

5.4. Drag forces for pitching and vertical motion with two degrees of freedom

Table 7 shows the performance of the different models that are tested on the 6 m/s two-degree-of-freedom random motion data. It can be seen that the Laguerrian filter basis performs best for the 3rd-order model, and overfitting for the 4th-order model is present. The 2nd-order model performs better than the linear model, but the performance is less than that for the 1DOF case. The 1st-order no-cross model is equal to the model with cross-terms because these models are equal. The 2nd$^-$ and 3rd-order models without cross-terms perform worse than the model with cross-terms. The 4th-order model without cross-terms gives less reduction in performance compared with the 4th-order model with cross-terms and can be an indication of overfitting due to a large number of unknown compared with the size of the training data. The $1+1$ DOF superposition data perform slightly worse than the linear models.

Fig. 17 shows the 1st-order kernel of the 2nd-order model with and without cross-terms. The 1st-order kernel of the 2nd-order model of the 1DOF data from the former chapter is also shown. In the figure, one can see that the vertical motion has slightly longer memory at approximately 50 terms compared with the 45 terms of the pitching motion. It is interesting to note that both the vertical and pitching motion 1st-order kernels are similar for the model with and without cross-terms. However, the 1st-order kernel of the 2nd-order model from the 1DOF test has significantly higher amplitudes compared to the 2DOF test. It seems that the model has a hard time extracting correct information from the model, and the model keeps treating the other motions as noise. Additional data could alleviate the problem. The size of the vertical motion 1st-order kernel is larger than the pitching motion kernel, indicating that the vertical motion has a more significant impact on the drag per unit of displacement.

Fig. 18 shows the 2nd-order kernels for the 2nd-order models with and without cross-terms. $h_{2,zz}$ and $h_{2,\theta\theta}$ are similar in shape for the cross- and no-cross-term models, but the amplitudes are different. The $h_{2,\theta z}$ and $h_{2,z\theta}$ could, in general, be equal, so a comparison between them is obsolete, but it appears that the memory of the cross-kernels is about the same lengths as the direct kernels.

Fig. 19 shows a time-domain realization of the different models. At time instances 255.8 and 260.1, one can observe that the 1+1DOF model struggles to predict forces when both vertical and pitching motion is at their negative peaks. The 2nd-order model with cross-terms performs fairly well, given that the model data are noisy and that the model has a limited amount of data. The performance of the model with cross-terms is better than the performance without cross-terms, indicating that the cross-term has an impact on the model, but the performance with cross-terms is significantly lower than the 1DOF problem displayed earlier.

6. Conclusion

In this paper, the use of parametrized functions called the Laguerrian expansion basis for identifying Volterra models is explored. Volterra models are used to predict nonlinear aerodynamic self-excited forces on twin decks. It is found that the parameterized Volterra kernels have several advantages: *i)* they have fewer unknown coefficients, which leads to a significantly less computationally expensive identification problem; *ii)* recursive relationships inherent to Laguerrian filters provide an opportunity for fast self-computation; *iii)* the kernels decay smoothly towards zero, and this suppresses high-order noise; *iv)* the memory length can be specified almost arbitrarily high without the addition of computational effort.

The method was used to identify kernels using experimental data from wind tunnel tests on a twin deck, and the following conclusions can be drawn:

- For the 1DOF motion problem, low filter orders were used, and good performance was observed. The 2nd-order models gave a slight increase in performance for nearly linear datasets but a significant increase for the nonlinear datasets. The 3rd-order models gave a small increase in performance, but the 4th-order model gave no increase over the 3rd-order models.
- The Volterra kernels gained from the technique were smooth and easily interpretable.
- For the 2DOF motion problem, the technique works well for slightly nonlinear datasets, but for more nonlinear and noisy datasets, such as the drag force, the performance decreased, but the performance was still better than the model without cross-terms and significantly better than linear and 1+1DOF models.

The capabilities of the method for efficient identification and modelling of nonlinear self-excited forces indicate that it could be applied to other nonlinear bridge aerodynamics phenomena. A natural extension, which remains to be further investigated, is the modelling of self-excited lift and moment at large angles of attack, which is of particular interest when evaluating the stability limit of long-span bridges. A limitation of the present work is that only vertical and pitching motion has been considered, but horizontal motion can also straightforwardly be used. It should however be acknowledged that it is difficult to obtain reliably experimental results for self-excited forces due to horizontal motion since the forces are small.

Moving forward, implementing the model in finite element software utilizing the model in response analysis for the full structure would be of interest.

Author statement

Henrik Skyvulstad: Conceptualization, Methodology, Software, Formal analysis, Writing - Original Draft, Visualization, Funding acquisition, Øyvind W. Petersen: Conceptualization, Methodology, Writing - Original Draft, Tommaso Argentini: Writing - Review & Editing, Alberto Zasso: Writing - Review & Editing, Ole Øiseth: Conceptualization, Methodology, Writing - Review & Editing, Supervision, Project administration, Funding acquisition.

Toolbox

The authors have supplied a MATLAB toolbox together with the manuscript.

Declaration of competing interest

The authors declare that they have no known competing financial interests or personal relationships that could have appeared to influence the work reported in this paper.

Acknowledgements

The research presented in this paper has been financed by Norconsult AS, The Norwegian Public Roads Administration (NPRA) and The Research Council of Norway grant nr. 263483.

Appendix A. Supplementary data

Supplementary data to this article can be found online at https://doi.org/10.1016/j.jweia.2021.104805.

References

Abbas, T., Kavrakov, I., Morgenthal, G., Lahmer, T., 2020. Prediction of aeroelastic response of bridge decks using artificial neural networks. Comput. Struct. 231 https://doi.org/10.1016/j.compstruc.2020.106198.

Ali, K., Katsuchi, H., Yamada, H., 2020. Numerical simulation of buffeting response of long-span bridges in time-domain using Volterra based wind load model. J. Struct. Eng. 66A, 292–302. https://doi.org/10.11532/structcivil.66A.292.

Amorocho, J., Brandstetter, A., 1971. Determination of nonlinear functional response functions in rainfall runoff processes. Water Resour. Res. 7, 1087–1101.

Batselier, K., Chen, Z., Wong, N., Bouvier, D., Hélie, T., Roze, D., Bouvier, D., Hélie, T., Roze, D., Bouvier, D., Hélie, T., Roze, D., Lin, R.M., Ng, T.Y., Kavrakov, I., Legatiuk, D., Gürlebeck, K., Morgenthal, G., de Paula, N.C.G., Marques, F.D., Wu, B., Chen, X., Wang, Q., Liao, H., Dong, J., 2019. Tensor Network alternating linear scheme for MIMO Volterra system identification. Nonlinear Dynam. 197, 487–516. https://doi.org/10.1098/rsos.181848.

Campello, R.J.G.B., Amaral, W.C., Favier, G., 2001. Optimal Laguerre series expansion of discrete volterra models. 2001 Eur. Control Conf. ECC 372–377. https://doi.org/10.23919/ecc.2001.7075935, 2001.

Campello, R.J.G.B., Do Amaral, W.C., Favier, G., 2006. A note on the optimal expansion of Volterra models using Laguerre functions. Automatica 42, 689–693. https://doi.org/10.1016/j.automatica.2005.12.003.

Campello, R.J.G.B., Favier, G., Amaral, W.C., 2003. Optimal expansions of discrete-time volterra models using laguerre functions. In: IFAC Proceedings Volumes (IFAC-PapersOnline), pp. 1807–1812. https://doi.org/10.1016/S1474-6670(17)35022-X.

Carassale, L., Kareem, A., 2010. Modeling nonlinear systems by volterra series. J. Eng. Mech. 136, 801–818. https://doi.org/10.1061/(ASCE)EM.1943-7889.0000113.

Carassale, L., Wu, T., Kareem, A., 2014. Nonlinear aerodynamic and aeroelastic analysis of bridges: frequency domain approach. J. Eng. Mech. 140, 1–14. https://doi.org/10.1061/(ASCE)EM.1943-7889.0000737.

Chen, X., Kareem, A., 2003. Aeroelastic analysis of bridges: effects of turbulence and aerodynamic nonlinearities. J. Eng. Mech. 129, 885–895. https://doi.org/10.1061/(ASCE)0733-9399(2003)129:8(885).

Chen, X., Kareem, A., 2001. Nonlinear response analysis of long-span bridges under turbulent winds. J. Wind Eng. Ind. Aerod. 89, 1335–1350. https://doi.org/10.1016/S0167-6105(01)00147-7.

Chen, Z., Tse, K.T., Kwok, K.C.S., Kim, B., Kareem, A., 2020. Modelling unsteady self-excited wind force on slender prisms in a turbulent flow. Eng. Struct. 202, 109855 https://doi.org/10.1016/j.engstruct.2019.109855.

Cheng, C.M., Peng, Z.K., Zhang, W.M., Meng, G., 2017. Volterra-series-based nonlinear system modeling and its engineering applications: a state-of-the-art review. Mech. Syst. Signal Process. 87, 340–364. https://doi.org/10.1016/j.ymssp.2016.10.029.

Clancy, S.J., Rugh, W.J., 1979. A note on the identification of discrete-time polynomial systems. IEEE Trans. Automat. Control 975–978.

Costa, C., Borri, C., 2006. Application of indicial functions in bridge deck aeroelasticity. J. Wind Eng. Ind. Aerod. 94, 859–881. https://doi.org/10.1016/j.jweia.2006.06.007.

Delport, R., 2005. Process Identification Using Second Order Volterra Models for Nonlinear Model Predictive Controll Design of Floatation Circuits. Univercity of Pretoria.

Denoël, V., Carassale, L., 2015. Response of an oscillator to a random quadratic velocity-feedback loading. J. Wind Eng. Ind. Aerod. 147, 330–344. https://doi.org/10.1016/j.jweia.2015.09.008.

Diana, G., Bruni, S., Cigada, A., Collina, A., 1993. Turbulence effect on flutter velocity in long span suspended bridges. J. Wind Eng. Ind. Aerod. 48, 329–342. https://doi.org/10.1016/0167-6105(93)90144-D.

Diana, G., Falco, M., Bruni, S., Cigada, A., Larose, G.L., Darnsgaard, A., Collina, A., 1995. Comparisons between wind tunnel tests on a full aeroelastic model of the proposed bridge over Stretto di Messina and numerical results. J. Wind Eng. Ind. Aerod. 54–55, 101–113. https://doi.org/10.1016/0167-6105(94)00034-B.

Diana, G., Omarini, S., 2020. A non-linear method to compute the buffeting response of a bridge validation of the model through wind tunnel tests. J. Wind Eng. Ind. Aerod. 201, 104163 https://doi.org/10.1016/j.jweia.2020.104163.

Diana, G., Resta, F., Rocchi, D., 2008. A new numerical approach to reproduce bridge aerodynamic non-linearities in time domain. J. Wind Eng. Ind. Aerod. 96, 1871–1884. https://doi.org/10.1016/j.jweia.2008.02.052.

Diana, G., Resta, F., Zasso, A., Belloli, M., Rocchi, D., 2004. Forced motion and free motion aeroelastic tests on a new concept dynamometric section model of the Messina suspension bridge. J. Wind Eng. Ind. Aerod. 92, 441–462. https://doi.org/10.1016/j.jweia.2004.01.005.

Diana, G., Rocchi, D., Argentini, T., 2013. An experimental validation of a band superposition model of the aerodynamic forces acting on multi-box deck sections. J. Wind Eng. Ind. Aerod. 113, 40–58. https://doi.org/10.1016/j.jweia.2012.12.005.

Diana, G., Rocchi, D., Argentini, T., Muggiasca, S., 2010. Aerodynamic instability of a bridge deck section model: linear and nonlinear approach to force modeling. J. Wind Eng. Ind. Aerod. 98, 363–374. https://doi.org/10.1016/j.jweia.2010.01.003.

Fu, Y., Dumont, G.A., 1993. An optimum time scale for discrete laguerre network. IEEE Trans. Automat. Control 38, 934–938. https://doi.org/10.1109/9.222305.

Gao, G., zhong, Zhu, dong, L., 2017. Nonlinear mathematical model of unsteady galloping force on a rectangular 2:1 cylinder. J. Fluid Struct. 70, 47–71. https://doi.org/10.1016/j.jfluidstructs.2017.01.013.

Gao, G., Zhu, L., Han, W., Li, J., 2018. Nonlinear post-flutter behavior and self-excited force model of a twin-side-girder bridge deck. J. Wind Eng. Ind. Aerod. 177, 227–241. https://doi.org/10.1016/j.jweia.2017.12.007.

Gao, G., Zhu, L., Li, J., Han, W., Yao, B., 2020. A novel two-degree-of-freedom model of nonlinear self-excited force for coupled flutter instability of bridge decks. J. Sound Vib. 480, 115406 https://doi.org/10.1016/j.jsv.2020.115406.

Han, Y., Liu, S., Hu, J.X., Cai, C.S., Zhang, J., Chen, Z., 2014. Experimental study on aerodynamic derivatives of a bridge cross-section under different traffic flows. J. Wind Eng. Ind. Aerod. 133, 250–262. https://doi.org/10.1016/j.jweia.2014.08.003.

Hayashi, K., Tsuda, N., Sawa, T., Hagihira, S., 2007. Ketamine increases the frequency of electroencephalographic bicoherence peak on the α spindle area induced with propofol. Br. J. Anaesth. 99, 389–395. https://doi.org/10.1093/bja/aem175.

Israelsen, B.W., Smith, D.A., 2014. Generalized laguerre reduction of the volterra kernel for practical identification of a MIMO system. Fuels petrochemicals div. 2014 - core program. Area 2014 AIChE spring meet. 10th Glob. Congr. Process Saf. 1, 496–504.

Khawar, J., Zhigang, W., Chao, Y., 2012. Volterra kernel identification of MIMO aeroelastic system through multiresolution and multiwavelets. Comput. Mech. 49, 431–458. https://doi.org/10.1007/s00466-011-0655-9.

Korenberg, M.J., 1987. Functional expansions, parallel cascades, and nonlinear difference equations. Adv. Methods Physiol. Syst. Model. 1, 221–240.

Korenberg, M.J., Hunter, W., 1990. The identification of nonlinear biological systems: Weiner kernel approaches. 1 Ann. Biomed. Eng. 18, 629–654.

Lee, Y.W., Schetzen, M., 1965. Measurements of the Wiener kernels of non-linear system by cross-correlation. Int. J. Control 2, 237–254.

Marmarelis, V.Z., 1993. Identification of nonlinear biological systems using laguerre expansions of kernels. Ann. Biomed. Eng. 21, 573–589. https://doi.org/10.1007/BF02368639.

Nelles, O., 2001. Nonlinear System Identification from Classical Approaches to Neural Networks and Fuzzy Models. Springer-Verlag, Berlin.

Ogura, H., 1986. Estimation of Wiener kernels of a nonlinear system of fast algorithm using digital Laguerre filters. In: 15th NIBB Conference, pp. 14–62.

Øiseth, O., Rönnquist, A., Sigbjörnsson, R., 2011. Time domain modeling of self-excited aerodynamic forces for cable-supported bridges: a comparative study. Comput. Struct. 89, 1306–1322. https://doi.org/10.1016/j.compstruc.2011.03.017.

Prazenica, R., 2002. Wavelet-based Volterra Series Representations of Nonlinear Dynamical Systems. University of Florida.

Reisenthel, P., 1999. Prediction of Unsteady Aerodynamic Forces via Nonlinear Kernel Identification. Williamsburg, Virginia(USA).

Rugh, W., 1981. Nonlinear System Theory. The Johns Hopkins Univercity press.

Schetzen, M., 1980. The Volterra and Wiener Theories of Nonlinear Systems. Dower, New York.

Seretis, C., Zafirioul, E., 1997. Nonlinear dynamical system identification using reduced Volterra models with generalized orthonormal basis functions. In: Proceedings of the American Controll Conference, Albuquerque, pp. 3042–3046.

Siedziako, B., Øiseth, O., 2018. Modeling of self-excited forces during multimode flutter: an experimental study. Wind Struct. An Int. J. 27, 293–309. https://doi.org/10.12989/was.2018.27.5.293.

Siedziako, B., Øiseth, O., Rønnquist, A., 2017. An enhanced forced vibration rig for wind tunnel testing of bridge deck section models in arbitrary motion. J. Wind Eng. Ind. Aerod. 164, 152–163. https://doi.org/10.1016/j.jweia.2017.02.011.

Skyvulstad, H., Argentini, T., Zasso, A., Øiseth, O., 2021. Nonlinear modelling of aerodynamic self-excited forces: an experimental study. J. Wind Eng. Ind. Aerod. 209 https://doi.org/10.1016/j.jweia.2020.104491.

Skyvulstad, H., Siedziako, B., Øiseth, O., 2017. An experimental study of self-excited forces for twin deck section models. In: EACWE. Liege.

Volterra, V., 1959. Theory of Functionals and of Integral and Intergrodifferential Equations. Dower, New York.

Watanabe, A., Stark, L., 1975. Kernel method for nonlinear analysis: identification of biological control system. Math. Biosci. 99–108.

Westwick, D., Kearney, R., 2003. Identification of Nonlinear Physiological Systems.

Wiener, N., 1958. Nonlinear problems in random theory. In: New York. Wiley.

Wray, J., Green, G., 1994. Calculation of the Volterra kernels of non-linear dynamic systems using an artificial neural network. Biol. Cybern. 71, 187–195.

Wu, T., Kareem, A., 2015a. A nonlinear analysis framework for bluff-body aerodynamics: a Volterra representation of the solution of Navier-Stokes equations. J. Fluid Struct. 54, 479–502. https://doi.org/10.1016/j.jfluidstructs.2014.12.005.

Wu, T., Kareem, A., 2015b. A low-dimensional model for nonlinear bluff-body aerodynamics: a peeling-an-onion analogy. J. Wind Eng. Ind. Aerod. 146, 128–138. https://doi.org/10.1016/j.jweia.2015.08.009.

Wu, T., Kareem, A., 2014. Simulation of nonlinear bridge aerodynamics: a sparse third-order Volterra model. J. Sound Vib. 333, 178–188. https://doi.org/10.1016/j.jsv.2013.09.003.

Wu, T., Kareem, A., 2013a. Bridge aerodynamics and aeroelasticity: a comparison of modeling schemes. J. Fluid Struct. 43, 347–370. https://doi.org/10.1016/j.jfluidstructs.2013.09.015.

Wu, T., Kareem, A., 2013b. A nonlinear convolution scheme to simulate bridge aerodynamics. Comput. Struct. 128, 259–271. https://doi.org/10.1016/j.compstruc.2013.06.004.

Wu, T., Kareem, A., 2013c. Vortex-induced vibration of bridge decks: volterra series-based model. J. Eng. Mech. 139, 1831–1843. https://doi.org/10.1061/(ASCE)EM.1943-7889.0000628.

Wu, T., Kareem, A., 2011. Modeling hysteretic nonlinear behavior of bridge aerodynamics via cellular automata nested neural network. J. Wind Eng. Ind. Aerod. 99, 378–388. https://doi.org/10.1016/j.jweia.2010.12.011.

Zhang, M., Xu, F., Wu, T., Zhang, Z., 2020. Postflutter analysis of bridge decks using aerodynamic-describing functions. J. Bridge Eng. 25, 1–13. https://doi.org/10.1061/(ASCE)BE.1943-5592.0001587.

Zhang, M., Xu, F., Ying, X., 2017. Experimental investigations on the nonlinear torsional flutter of a bridge deck. J. Bridge Eng. 22, 1–22. https://doi.org/10.1061/(ASCE)BE.1943-5592.0001082.

Zhou, R., Ge, Y., Yang, Y., Du, Y., Liu, S., Zhang, L., 2019a. Nonlinear behaviors of the flutter occurrences for a twin-box girder bridge with passive countermeasures. J. Sound Vib. 447, 221–235. https://doi.org/10.1016/j.jsv.2019.02.002.

Zhou, R., Ge, Y., Yang, Y., Du, Y., Zhang, L., 2018a. Wind-induced nonlinear behaviors of twin-box girder bridges with various aerodynamic shapes. Nonlinear Dynam. 94, 1095–1115. https://doi.org/10.1007/s11071-018-4411-y.

Zhou, R., Ge, Y., Yang, Y., Liu, S., Du, Y., Zhang, L., 2019b. A nonlinear numerical scheme to simulate multiple wind effects on twin-box girder suspension bridges. Eng. Struct. 183, 1072–1090. https://doi.org/10.1016/j.engstruct.2018.11.040.

Zhou, R., Yang, Y., Ge, Y., Zhang, L., 2018b. Comprehensive evaluation of aerodynamic performance of twin-box girder bridges with vertical stabilizers. J. Wind Eng. Ind. Aerod. 175, 317–327. https://doi.org/10.1016/j.jweia.2018.01.039.